2017

Modelling and Observational Evidence for the Igneous Evolution of the Elysium Volcanic Province on Mars

David Andrew Susko
Louisiana State University and Agricultural and Mechanical College

MODELING AND OBSERVATIONAL EVIDENCE FOR THE IGNEOUS EVOLUTION OF THE ELYSIUM VOLCANIC PROVINCE ON MARS

A Thesis

Submitted to the Graduate Faculty of the
Louisiana State University and
Agricultural and Mechanical College
in partial fulfillment of the
requirements for the degree of
Master of Science

in

The Department of Geology and Geophysics

by
David A. Susko
B.S., Louisiana State University, 2015
B.A., Louisiana State University, 2015
August 2017

Acknowledgements

First and foremost, I would like to thank my co-authors who helped me advance the first chapter of this thesis to the level of a peer-reviewed manuscript. My co-authors include Dr. Suniti Karunatillake, Dr. J.R. Skok, Dr. James Wray, Dr. Agnes Cousin, Dr. Jennifer Heldmann, Gayantha Kodikara, and Taylor Judice. I would like to acknowledge the NASA Mars Data Analysis Program (MDAP) grant NNX13A198G, the LA Space Grant Consortium REA grant 115-40-4139, and the LA Space Grant Consortium Graduate Student Research Award (GSRA) without which none of this research would have been possible. I would also like to acknowledge *Scientific Reports* as the journal and Alberto G. Fairén as the editor who facilitated the peer-reviewed process for the publication of this chapter. Thank you to the reviewers of this manuscript Dr. James Dohm and a second reviewer who wished to remain anonymous. Also, thank you Charles Everhardt and Rory Bentley for their hard work with crater counting, and to Lorrie Carnes and Don Hood for providing editorial revisions.

For the second chapter of the thesis, I would like to thank Don Hood for writing the Python code used in the extraction of data from the pMELTS results and exporting them into an easy to use spreadsheet. I would like to thank Dr. Antonio Genova for providing the map of martian crustal thicknesses used in the interpretation section of this paper. Last, I would like to thank Dr. Darrell Henry for providing the tools for learning how to operate the pMELTS thermodynamic calculator.

Table of Contents

List of Tables

List of Figures

Abstract

A major knowledge gap exists on how eruptive compositions of a single martian volcanic province change over time. The Elysium Volcanic Province is a location of great geologic interest on Mars. Its predominantly Amazonian surface age (beginning 3.3 Ga), and its isolation in the northern hemisphere of Mars away from other volcano-tectonic regions, make it an ideal locale to investigate igneous compositions erupted during the most recent geologic period on Mars. Here, this work seeks to fill that gap by assessing the compositional evolution of Elysium as a major martian volcanic province in two related projects. The first project seeks to characterize and contrast different portions of the Elysium Volcanic Province chronologically, morphologically, and geochemically, to establish evidence for spatio-temporal magmatic evolution across the province. This study is additional motivated by a unique geochemical signature which overlaps with the southeastern flows of this volcano. The geochemical and temporal differences between the SE and NW lava fields are interpreted to be consistent with primary magmatic processes, such as a change in depth of melt formation within the martian mantle due to crustal loading and lithospheric flexure. In the second project, the petrologic modeling software pMELTS is used to simulate the partial melting of the martian mantle. By using a range of possible initial conditions and comparing the corresponding model outcomes to geochemistry on the surface --as derived from the Gamma-ray and Neutron Spectrometer (GRS)-- the mantle conditions of the magma source are constrained for each portion of the Elysium Volcanic Province. The geochemistry of the Elysium Volcanic Province is consistent with liquid compositions produced by 10-20% partial melting for all three sub-regions and pressures are estimated to be between 17 and 21 kbars for Central Elysium, between 17 and 19 kbars for NW Elysium, and between 14 and 16 kbars for SE

Elysium. These pressures correspond to depths of melt formation that are consistent with independently calculated thicknesses of the Elysium lithosphere.

Introduction

The lava fields surrounding Elysium Mons and its neighboring super-shield volcanoes, Albor Tholus and Hecates Tholus (Figure 1), record some of the most recent volcanism on Mars [*Hartmann and Berman*, 2000; *Dohm et al.*, 2008; *Karunatillake et al.*, 2009; *Baratoux et al.*, 2011]. The Elysium lava flows erupted from the edifices of the three super-shields, from volcanic fissures, and from at least 22 topographically low shield volcanoes scattered across the Elysium Volcanic Province [*Vaucher et al.*, 2009]. Most of the surface of the Elysium Volcanic Province dates to the Amazonian period[*Grott et al.*, 2012; *Tanaka et al.*, 2014a, 2014b], (beginning between 3.3 and 2.9 Ga), with a considerable areal extent of Late Amazonian age (beginning 0.6 to 0.3 Ga [*Hartmann and Berman*, 2000]). Past work estimates that the age of the basement lava flows, the stratigraphically lowest and oldest visible in the region, date to ~4 Ga [*Hartmann and Berman*, 2000]. Other studies have identified late periods of volcanic activity in isolated areas of the southern portion of the Elysium Volcanic Province to extend to the last 250 Ma, including some remarkably young episodes as recent as 16.2-13.5 Ma, 4.3 Ma, and 3-2.5 Ma [*Vaucher et al.*, 2009]. These dates highlight the Elysium Volcanic Province as particularly interesting, given its long and continuous history of volcanic activity. This long history suggests that these lavas could record varied magmatic evolution that can provide important constraints on the evolution of Mars as a geologically active and diverse planet. The Elysium Volcanic Province may also provide important insight into the geologic evolution of Amazonian terrains, given its geographic isolation in the northern lowlands away from other volcano-tectonic regions.

In this thesis, two separate, but related projects seek to quantify the magmatic evolution of the Elysium Volcanic Province. In the first, remote sensing observations from a range of instruments including the Gamma- and- Neutron Ray Spectrometer (GRS), the High-Resolution Imaging

Science Experiment (HiRISE), and The Mars Orbiting Laser Altimeter (MOLA) are used together with in-situ observations from the Mars Exploration Rovers (MER) and laboratory assessment of martian meteorites in order to quantify, compare, and analyze the geology of the volcanic province.

Geochemistry from the GRS provides insight into the various geologic process who could be influencing the composition of the surface down to decimeter scale depths. This work investigates the possibility of both igneous and non-igneous influences in the region. Suggesting the possibility of a dominance of fine grained "dust" material dominated the top most layer of the martian surface or aqueous alteration from the presence of repeated flooding from outflow channels in the southeast potion of the province. Several magmatic models are also proposed, suggesting either the presence of a heterogeneous mantle or a change in the depth of melt formation for the magma source. After analyze the data, this work determines the most likely model is a change in depth of melting due to lithospheric loading.

The second chapter of this thesis extents its analysis into petrologic modeling of the mantle beneath the Elysium Volcanic Province. Through simulations of basaltic crystallization of melt under various temperature and pressure conditions, this work seeks to support the conclusions of the first chapter. By using the pMELTS software, this work simulates the conditions for Elysium during the time of the resurfacing events which are seen on the surface of Mars today. Surfaces of variable age are compared against the results of pMELTS and source conditions are estimates for each sub-region, allowing a chronological interpretation of how the volcanic province change from the Late Hesperian to the Late Amazonian eras. The results from this study are consistent with the proposed model from the interpretations of Chapter One.

Chapter 1: A Record of Igneous Evolution in Elysium, A Major Martian Volcanic Province

1.1 Introduction

Mid-latitude (exclude latitudes poleward of ~±45˚) mapping of mass fraction distributions of the 9 elements Al, Ca, Cl, Fe, H, K, Si, S, Th, obtained from the γ spectral data from the Mars Odyssey Gamma and Neutron Spectrometer (GRS) instrument suite [*Boynton et al.*, 2007; *Feldman et al.*, 2007; *Karunatillake et al.*, 2009; *Gasnault et al.*, 2010; *Taylor et al.*, 2010; *Gaillard et al.*, 2012], showed a unique geochemical signature for Amazonian lava flows [*Karunatillake et al.*, 2009] in the southeastern portion of the Elysium volcanic province (Figure 1). This sub-region of the encompassing Volcanic Province extends from 25˚N down to the equator of the planet and includes both the massive volcanic edifice of the super shield Albor Thous and a segment of the nearby Tartarus Montes. Work by Karunatillake *et al*. [2009] identified depletions in both K and Th (two elements characterized by the strongest geochemical affinity during igneous processes [*Taylor et al.*, 2006; *Gasnault et al.*, 2010]) by more than the combined standard deviation and typical standard error relative to their respective global averages. The major depletions in these elements indicate that the southeastern lava fields are chemically anomalous to decimeter depth scales when compared to the compositions of the martian mid-latitudinal regolith [*Boynton et al.*, 2007]. These anomalous geochemical signatures identify the Southeast Elysium lava fields as promising candidates for further geochemical investigation.

Another portion of the Elysium Volcanic Province lies directly to the northwest, adjacent to The Southeast Elysium sub-region. Baratoux *et al.* [2011] used the Northwest Elysium lava fields (Figure 1) to investigate the thermal history of Mars during the Amazonian period. This sub-region is smaller than the Southeast, but includes the volcanic edifices of the super shields Elysium Mons and Hecates Tholus. These authors investigated the composition of the lavas using γ data

from the GRS instrument and compared it to the compositions of various Hesperian and Amazonian volcanic provinces across the surface of Mars [*Baratoux et al.*, 2011]. Abundances of SiO_2, FeO and Th were used to estimate mantle potential temperature, degree of partial melting, and lithospheric thickness in correspondence with these volcanic provinces when these eruptions

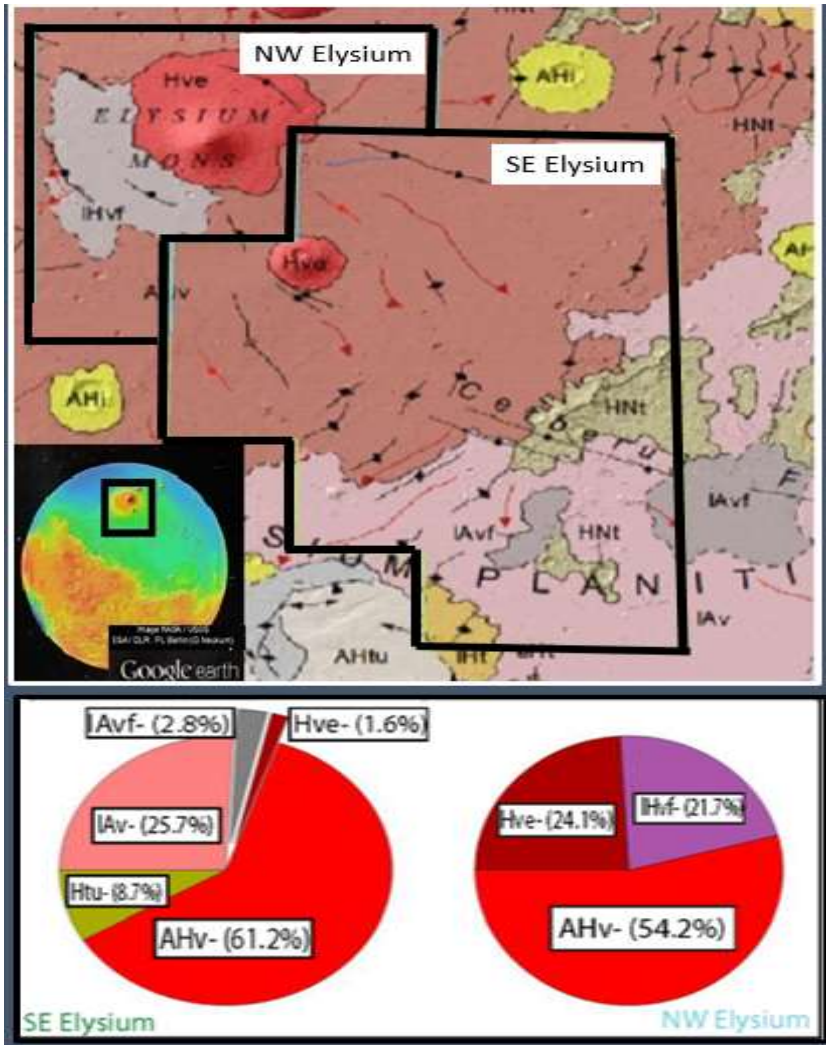

Figure 1. Location and geological setting of the Southeast (Green) and Northwest (Blue) Elysium lava fields with corresponding GRS pixels. Geology map adopted from the work by Tanaka et al.*[2014a]* and made publicly available at http://pubs.usgs.gov/sim/3292/pdf/sim3292_map.pdf. Inset image is a global reference map for Mars with overlain MOLA topography from Google Earth. The areal fraction of each unit within each region is quantified using ArcGIS software (pie charts). AHv is"Amazonian and Hesperian Volcanic unit", lAv is "Late Amazonian Volcanic unit", lAvf is "Late Amazonian Volcanic field unit", lHvf is "Late Hesperian Volcanic Field unit", Hve is "Hesperian volcanic Edifice unit", Htu in the pie charts stands for "Hesperian Transition units" and is a combination of 3 geologic units: HNt (Hesperian- Noachian transition unit), lHt (Late Hesperian transition unit), and AHtu (Amazonian-Hesperian transition unit). North is up in this geologic map.

took place [*Baratoux et al.*, 2011]. The results from this work were used to infer a cooling rate and lithospheric thickening for Mars on the global scale.

The geochemical anomalies which exist in within the southeast sub-region of the Elysium Volcanic Province motivate the investigation into several igneous and non-igneous processes which have been described by prior work. One such possibility is interference from a thick layering of dust influencing GRS compositions. Mars has a history of global-scale dust storms which mobilize layers of high albedo fine material of few μm to tens of μm size scale (i.e., dust) across the planetary surface [*Spohn, T., Breuer, D. & Johnson*, 2014]. Elysium in particular has a thick layer of this dust [*Ruff and Christensen*, 2002].

Another non-igneous model involves repeated aqueous flooding of the Cerebus Fossae [*Burr et al.*, 2002a], which could lead to aqueous alteration of surface compositions in the SE sub-region. The surrounding area contains evidence of chemical layering involving volatile elements in the subsurface, potentially due to complex interactions among lava flows, volcanic aerosols and eolian sediment [*Diez et al.*, 2009]. Morphologies, such as mesas and other related features in close proximity to Cerberus Fossae, have been ascribed to phreatomagmatism [*Burr et al.*, 2002b; *Jaeger et al.*, 2007; *Dohm et al.*, 2008], lava-water interactions [*Burr et al.*, 2002a] and relict ice floes [*Murray et al.*, 2005; *Page*, 2008]. Observations of patterned ground with a remarkable similarity to terrestrial periglacial environments [*Balme et al.*, 2009] also suggest the likelihood of geologically recent aqueous processes. All these processes could explain some of the observed chemistry. However, radar sounding data appear consistent with interbedded lava flows and weakly compacted sediments or porous rocks [*Morgan et al.*, 2015].

Pure water is unstable on the surface of Mars [*Chevrier and Altheide*, 2008; *Altheide et al.*, 2009; *Chevrier and Rivera-Valentin*, 2012]. Brines, however, could have been free-flowing on the

surface and could still be present in subsurface reservoirs of Mars [*Ojha et al.*, 2015], and thus could be thought of as agents for alteration of surface rock. Common secondary minerals on Mars, such as Ca- and Mg- Sulfates and Fe-Oxides could be deposited by low pH, sulfur-rich, aqueous solutions in very low water-to-rock ratio, and subsequently, limited Al-mobilization conditions [*Hurowitz and McLennan*, 2007]. Evaporite minerals, such as Halite (NaCl) and anhydrite ($CaSO_4$) could have precipitated following evaporation of highly saline aqueous solutions. If the volatiles detectable by the GRS, (S, Cl, and H_2O) are enriched in either SE or NW Elysium, this could support the presence of such minerals at regional scales.

Several igneous models of magmatic evolution involve changes in mantle structure and composition throughout time. Balta and McSween [2013b Figure 3] presents an igneous evolution model which might be applied in the regional context of Elysium. By analyzing Amazonian-aged Shergottites, meteorites which may represent hydrated, mafic to ultramafic martian crustal material, Balta and McSween [2013b] developed a model of magmatic evolution for Mars from the Noachian to the Amazonian. The Amazonian is described to have occasional upwelling of magma from a deep, H_2O-rich mantle which contains hydrous reservoirs [*Balta and McSween*, 2013b].

In this work, both the Southeast (SE) Elysium region and the Northwest (NW) Elysium region are characterize chronologically, using mapped geology and crater counting, and geochemically, using the data from the GRS instrument. They are then compared to constrain the spatial and temporal variation of composition of lava flows across the Elysium Volcanic Province. This comparison is used to quantify how the two sub-regions compare in the elemental compositions which made the SE sub-region notably anomalous. This work seeks to establish evidence for an origin of the anomalous chemistry observed by Karunatillake et al. [2009] in the SE. Through

analysis, this work rules out the presence of a non-igneous geochemical signature, such as those that form from aqueous alteration or interference from aeolian dust. Rather, igneous processes are suggested as the principal factor controlling Elysium's anomalous compositions.

1.2 Methods

In order to investigate a potential sub-era variation in volcanism, mapped geologic units in the SE and NW Elysium chemical provinces [*Tanaka et al.*, 2014a, 2014b] and crater counting techniques are used to estimate crustal ages for each area. ArcGIS software in conjunction with the Mars Orbiter Laser Altimeter (MOLA) data is used to highlight the areas of interest. These highlighted areas are saved as shape files and delineated these shape files based on mapped geology. The percentage of the surface dominated by each rock type is quantified in Figure 1. Within each area, craters are marked by defining three points around the rim. Each file is then exported them to the CraterStats2 program, which generates a crater diameter vs. cumulative crater frequency graph (Figure 3) and calculates the estimated ages for the two provinces [*Hartmann and Neukum*, 2001].

In the present work, the data from all γ pixels in the martian mid-latitudes, other than those identified as the Elysium Volcanic Province, collectively represent the bulk composition of the martian crust, down to depths of several decimeters [*Taylor*, 2013]. Each GRS pixel has a spatial resolution of several hundred-square kilometer. The relatively small size of the area of Mars occupied by the Elysium chemical provinces also ensures that other data pixels approximate the bulk crust characterized before by Taylor *et al.* [2006] and McSween *et al.* [2009]. Specifically, while the extent of the SE and NW Elysium chemical provinces (Figure 1) are roughly 1.37 $x10^6$ km^2 and 5.06 $x10^5$ km^2, respectively, they constitute a sufficiently small area to ensure that their exclusion from the bulk crustal values does not make the bulk crustal estimate unreliable.

For investigations using the γ data, this work uses the maps constructed from cumulative γ-spectra mapping periods extending through 2009, refining the older compositional data for greater accuracy and precision that those used in Karunatillake *et al.*[2009]. This work also includes previously unreported chemical maps for the elements Al and S. The chemical data exclude latitudes poleward of ~±45˚, where high H concentrations cause both mass dilution effects and inaccuracies in γ spectrum-to-elemental mass fraction derivation [*Boynton et al.*, 2007; *Karunatillake et al.*, 2009]. This work uses mid-to-low latitudinal mass fraction maps generated from the GRS instrument. Each of the maps is binned from their original dimensions to 5˚×5˚ pixel size. This reduces uncertainty associated with the reduced degrees of freedom from spatial autocorrelation [*Karunatillake et al.*, 2011, 2012]. The radioactive elements K and Th are the two elements with the finest γ spatial resolution, owing to the orbiting instrument's detection of natural radioactive decay and independence from neutron-driven scatter and capture processes, unique among the majority of elements detected by the GRS instrument [*Boynton et al.*, 2007]. It is for this reason that K and Th are the primary elements used for interpretation of geologic processes.

While the primary data sets used for this work are the chemical maps derived from the γ-spectra of the GRS instrument, previous investigations in the Radar Stealth region [*Karunatillake et al.*, 2009] suggests that data from the High Resolution Imaging Science Experiment (HiRISE), on board the Mars Reconnaissance Orbiter (MRO), can lead to inferences about the physical properties of surface-to-subsurface material. This work uses HiRISE imagery to complement the interpretation of geochemical signatures.

To complement observations made by orbiting spacecraft, this work makes comparisons between the regional chemistry in Elysium and in-situ samples analyzed from rover landing sites on Mars and the martian meteorites. The compositional data for several martian meteorites as well

as in-situ samples from Gusev Crater, analyzed using the Alpha Particle X-ray Spectrometer (APXS) onboard the MER Spirit Rover, are used for comparison with the γ data. The martian meteorites, which have been used in the past to model the compositions for bulk silicate Mars [*Dreibus and Wanke*, 1985; *Taylor*, 2013], provide the most detailed information about the martian mantle's evolution and magmatic differentiation of any data set available to us. The meteorites used in the analysis of this project are listed in Table 1 along with a classification based on rock type and composition. In order to better understand igneous alteration trends, which may be applicable to the Elysium Volcanic Province, this work uses previously categorized in-situ rock samples from Gusev, which have been divided into unaltered and altered igneous samples [*Hurowitz et al.*, 2006; *McSween et al.*, 2008; *Ming et al.*, 2008; *Karunatillake et al.*, 2010].

Ratio bound box plots show meaningful differences in compositional distributions between the SE and NW regions. In the ratio bound box plot method, the ratio of the 25th percentile of a particular element's reported mass fraction within a region "A" to the 75th percentile of values for the same element within a region "B" would bound how low the values are within "A" relative to those present within "B". The ratio of the 25^{th}%tile of "A"/75^{th}%tile of "B" is represented by the bottom of each "box" in Figure 4. Likewise, the ratio of the 75th percentile of region "A" compared to the 25th percentile within "B" bounds how high the values within "A" can be relative to those within "B". The ratio of the 75^{th}%tile of "A"/25^{th}%tile of "B" is represented by the top of each "box" in Figure 4. The ratio of the 50th percentile of "A" to the 50th percentile of region "B" (ratio of medians) indicates how the typical compositions compare with one another, represented in the

Table 1. Listed all the meteorites with previous chemical analysis completed and stored on NASA's Martian Meteorite Compendium (http://curator.jsc.nasa.gov/antmet/mmc/). 42 meteorites have been divided into 8 descriptive types, and the number of each type is listed in the right-hand column.

Description	Sample Name	# of Meteorites
Basaltic Shergottite	EET 79001B, Shergottty, QUE94201, Zagami, Los Angeles, NWA 480, NWA 5298, NWA 4342	8
Depleted Olivine-Phyric Shergottite	NWA 4925, NWA 4789, NWA 5590, NWA 6162	4
Olivine Phyric Shergottite	EET 79001A, Dar Al Gani 476, Dhofar 019, Dhofar 378, LAR 06319, NWA 1068, NWA 2990, NWA 6234, NWA 4480, RBT 04262, SaU, Y980459	12
Lherzolitic Shergottite	ALH 77005, LEW 88516, Y793605, Grove Mountains 99027, NWA 1950, NWA 4797	6
Brecciated Shergottite	NWA 7034	1
Nakhlite	G Valadares, Lafayette, Nakhla, NWA 817, NWA 998, Y000593, MIL 03346, NWA 5790,	8
Orthopyroxenite	ALH 84001	1
Chassignite	Chassigny, NWA 2737	2
		42

mid-section of each "box". The error bars were propagated for the ratio of the 50th%tile/50th%tile using the median absolute deviations (MAD) for each element in both regions, using the equation MAD=median [|X_i-median (X_i)|], where median (X_i) is the median of all values in X_i. These error bars are statistically robust and typically overcompensate the uncertainty of the values of various %tiles. In this work, an elemental abundance in a region "A" is refered to as a "major" enrichment or depletion, relative to a region "B", when the lower (25th%tile/75th%tile) or upper (75th%tile/25th%tile) bound, respectively, surpasses unity. In turn, the enrichment or depletion is considered "minor" when the ratio of medians surpasses unity but the lower or upper bounds do not. An abundance is considered similar between the two regions if the ratio of the 50th%tile/50th%tile is within one standard error.

The derived chemical maps from the γ data are limited to the 9 elements mentioned previously. For our geochemical analysis, these elements are converted to their oxide wt% equivalent. Unfortunately, missing from the derived maps are several major and minor rock forming elements that can be very informative of the igneous processes, namely: Mg, Mn, Ti, Na, and P. In order to build a more complete picture of the regional geochemistry in the Elysium Volcanic Province, a method established by Baratoux et al. [2014] is used to calculate an estimated value for these elements for each GRS pixel. The method for MgO abundance calculation in this study uses the ratio between various oxides ratios reported in basaltic shergottite martian meteorites to calculate values for the following oxides: TiO_2, Na_2O, P_2O_5, and MnO (Table 2). Their calculated values are then added to the oxide values derived from the γ-spectral data from the GRS (Al_2O_3, CaO, FeO, SiO_2, and K_2O) and normalized each oxide to be [H_2O] and [Cl]-free. In this method, Baratoux et al. [2014] neglects SO_4 since S does not substantially contribute to the density of rock in the martian crust and all martian meteorites which have been analyzed have been S-free. S on the martian surface is assumed to be nearly completely derived from volcanic aerosols and not the basaltic lava flows. This work follows the same method to maintain consistency with the work by Baratoux et al. [2014]. The total sum of the wt % oxides (Al_2O_3, CaO, FeO, SiO_2, K_2O, Na_2O, TiO_2, P_2O_5, and MnO) was subtracted from 100, and the remaining value was assumed to represent the MgO content, as Mg is the only remaining major rock forming element. This process produces physically possible and realistic values for MgO in the martian crust. It is worth noting that uncertainties are very large for this calculation. To partially address these concerns, this work ignores any GRS pixels for which these calculations return Mg# <40 or >70, as it is not consistent with an igneous crust from an initial mantle composition of roughly Mg# 75 [*Dreibus and Wanke*,

1985; *Baratoux et al.*, 2014]. The Mg# was calculated by using the mole fraction of the oxides MgO and FeO with the formula [Mg#=100*(MgO/(MgO+FeO))].

Table 2. Table of ratios of incompatible elements in Basaltic Shergottite meteorites, taken from Baratoux et al. [2014].

Ratio	Na2O/TiO2	TiO2/P2O5	MnO/FeO	P2O5/K2O
SNC	1.374	1.151	0.025	4.297
Error	0.337	0.265	0.001	0.939

In addition to observations made by orbiting spacecraft, this work makes comparisons between the regional chemistry in Elysium and in-situ samples analyzed from rover landing sites on Mars and the martian meteorites. The compositional data for several martian meteorites as well as in-situ samples from Gusev Crater, analyzed using the Alpha Particle X-ray Spectrometer (APXS) onboard the MER Spirit Rover, are used for comparison with the γ data. The martian meteorites, which have been used in the past to model the compositions for bulk silicate Mars [*Dreibus and Wanke*, 1985; *Taylor*, 2013], provide the most detailed information about the martian mantle's evolution and magmatic differentiation of any data set available to us. In order to better understand igneous alteration trends, which may be applicable to the Elysium Volcanic Province, this work uses previously categorized in-situ rock samples from Gusev, which have been divided into unaltered and altered igneous samples [*Hurowitz et al.*, 2006; *McSween et al.*, 2008; *Ming et al.*, 2008; *Karunatillake et al.*, 2010].

The oxide data used in the construction of the geochemical ternary plot for the martian meteorites were obtained by previous studies in laboratory settings. They were accessed online from the publicly available Martian Meteorite Compendium (http://curator.jsc.nasa.gov/antmet/mmc/). Similarly, the in-situ samples analyzed with the Alpha Particle X-ray Spectrometer (APXS) by the MER rovers (Spirit) at Gusev Crater were obtained

online, publically available at MERAnalyst, (https://an.rsl.wustl.edu/), part of NASA's Planetary Data Systems interface.

1.3 Results

Using the most recent mapped geologic units of Mars [*Tanaka et al.*, 2014a, 2014b], this work quantifies the areal fraction of each geologic unit comprising both NW and SE Elysium (Figure 1). The SE Elysium region ($1.37x10^6$ km^2 in areal extent) is dominated by Amazonian volcanic units, which comprise nearly 90% ($1.23x10^6$ km^2) of its areal fraction. The most abundant unit type is the Amazonian-Hesperian volcanic unit (AHv), making up more than 60% ($8.22x10^5$ km^2) of the surface (Figure 1). The AHv contains low viscosity flood lavas and stacked, gently sloping, lobate flows of highly variable ages, which are sourced from vent systems and local fissures rather than large volcanic edifices [*Tanaka et al.*, 2014a]. Late Amazonian volcanic units and volcanic fields, lAv and lAvf, respectively, make up nearly 30% ($4.11x10^5$ km^2). They contain planar deposits consisting of troughs, ridges, and platy textures which are identified in HiRISE image Figure 2f. These units are young, and they include pristine flows and occasional sinuous lava channels (Figure 2d). The rest of the region is made up of Hesperian transition units (Htu) and the Hesperian Volcanic Edifice (HVe) of the super-shield Albor Tholus [*Tanaka et al.*, 2014a] (Figure 1).

Several Hesperian geologic units are mapped in the NW region of Elysium ($5.06x10^5$ km^2 in areal extent) [*Tanaka et al.*, 2014a, 2014b]. While the majority of the region is characterized as AHv (~54% of the surface, or $2.72x10^5$ km^2), a significant portion (~22% or $1.11x10^5$ km^2) of the surface is covered by the Late Hesperian volcanic field unit (lHvf). The lHvf unit is hundreds of meters thick and is made up of far flowing, low viscosity lavas which are locally modified by troughs and fissures [*Tanaka et al.*, 2014a], such as those shown in Figure 2c. The remaining ~24%

of the NW region ($1.21x10^5$ km^2) is covered by the HVe unit (~24%), which makes up the edifice of the super-shield volcano Elysium Mons [*Tanaka et al.*, 2014a]. These Hesperian units, which did not experience the same Amazonian volcanic resurfacing events as SE Elysium, contribute substantially to the observed geochemistry in the NW region.

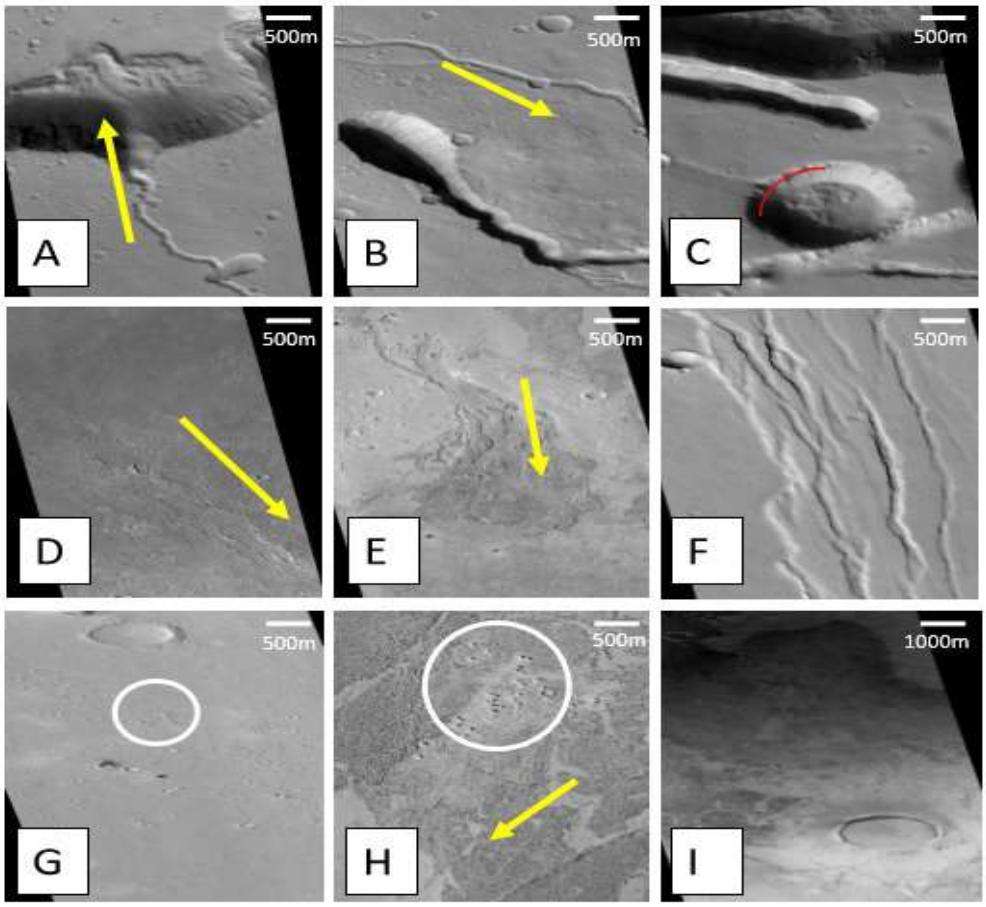

Figure 2. HiRISE imagery from both SE and NW Elysium regions. (A) ESP_022915_2070 (26.9˚N, 142.8˚E) flows down a crater slope in NW Elysium. (B) ESP_013157_2015 (21.5˚N, 149.7˚E) lava flows on the south flank of Elysium Mons within NW Elysium. (C) PSP_004046_2080 (27.5 ˚N, 143.2˚E) fissures and pit crater collapse feature of lava tubes in the NW region. The collapse of the lava tube has exposed stratified lava flows. (D) ESP_037802_1880 (8.1˚N, 154.7˚E) lava channels and accompanying lava levees within SE Elysium. (E) PSP_005984_1850 (5˚N, 156.4˚E) shows pa'hoe'hoe style flows and a lava-draped channel at its terminus within SE Elysium. (F) ESP_014278_2050 (24.7˚N, 143.6˚E) the lava flow boundary between separate geologic units HVe and lHvf in the NW region. (G) ESP_028466_1955 (15.2˚N, 162.5˚E) image from the SE with an infilled crater in the top half of the image and rootless cones (circled) in the bottom half. (H) ESP_012524_1855 (5.6˚N, 153.1˚E) rootless cone structures and Pa'hoe'hoe analog style flows within SE Elysium. (I) ESP_034967_1885 (8.5˚N, 149.2˚E) a large crater infilled by the lava flows from SE Elysium. North is up in all pictures. The yellow arrows represent inferred direction of flows.

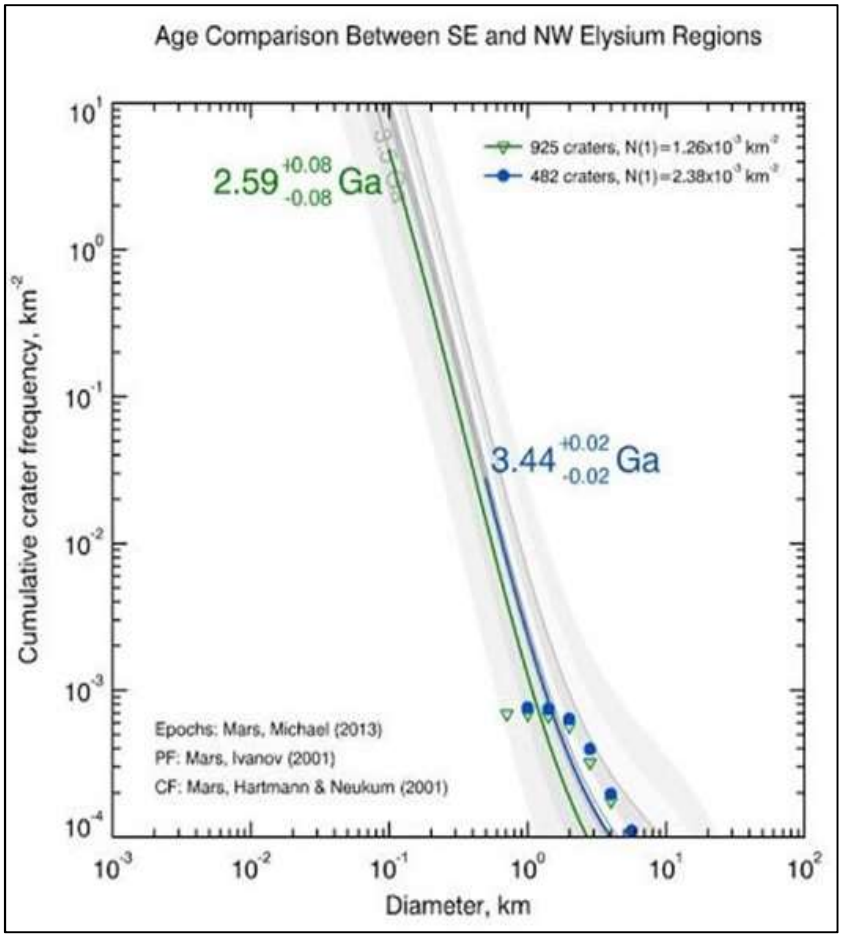

Figure 3. CraterStats2 results for planetary surface age dating using crater counting [Rogers and Nazarian, 2013; Tanaka et al., 2014b]. 925 craters greater than 1 km in diameter were identified for the SE Elysium region, while only 482 craters of the same size were identified in the smaller NW region. This figure plots Diameter of Craters vs Cumulative Crater Frequency. Southeast Elysium (green) is estimated to be younger at 2.59 ± 0.08 Ga and Northwest Elysium (blue) older at 3.44 ± 0.02 Ga.

While past analysis considered the ages of Elysium Planitia broadly [*Hartmann and Berman*, 2000], or on a more localized basis [*Vaucher et al.*, 2009; *Jaeger et al.*, 2010], this work sought to estimate the average age of all the lava flows within surface areas of similar regional geochemistry within Elysium [*Karunatillake et al.*, 2009; *Baratoux et al.*, 2011]. The total number of craters (N) greater than 1 km in diameter was found to be N=925 for the SE Elysium region and N=482 for the NW. The cumulative crater frequency reveal that the average age of the surface in SE Elysium province is 2.59 ± 0.08 Ga, while the surface in NW Elysium is estimated to be 3.44

± 0.02 Ga (Figure 3). Both dates are comparable to previous studies of the ages of various lava flows within Elysium, which estimated the oldest lava flows to range between 4 and 2 Ga [*Hartmann and Berman*, 2000].

Ratio bound box plots [*Karunatillake et al.*, 2009] show meaningful differences in compositional distributions between the SE and NW regions. In this work, an elemental abundance in a region "A" is refered to as a "major" enrichment or depletion, relative to a region "B", when the lower (25^{th}%tile/75^{th}%tile) or upper (75^{th}%tile/25^{th}%tile) bound, respectively, surpasses unity. In turn, the enrichment or depletion is considered "minor" when the ratio of medians surpasses unity but the lower or upper bounds do not. An abundance is considered similar between the two regions if the ratio of the 50^{th}%tile/50^{th}%tile is within one standard error. The error-bound median ratio are listed in parenthesis following the element.

The first ratio bound box plot compares the regional geochemistry of the SE Elysium region to the composition of the average martian crust (Figure 4a). In addition to the previously identified major depletions of K (0.72±0.05) and Th (0.63±0.05) [*Karunatillake et al.*, 2009], this region differs significantly from the typical martian crust in several elements detectable with γ spectra, as shown by Figure 4a. The region has a minor depletion in Si (0.97±0.02) and Al (0.91±0.05), while Ca (1.26±0.10) and Fe (1.11±0.08) display major enrichments throughout the region. For example, the lowest values, represented in the 25th percentile, of Ca and Fe, exceed most of the highest values, represented in the 75th percentile, of the martian crust. This amounts to concentrations of Fe over 16% of the bulk composition in some parts of the region, which is significant, considering that average for the martian crust is only 12.6 ± 0.7%. A major regional enrichment in S (1.14±0.04) is also observed.

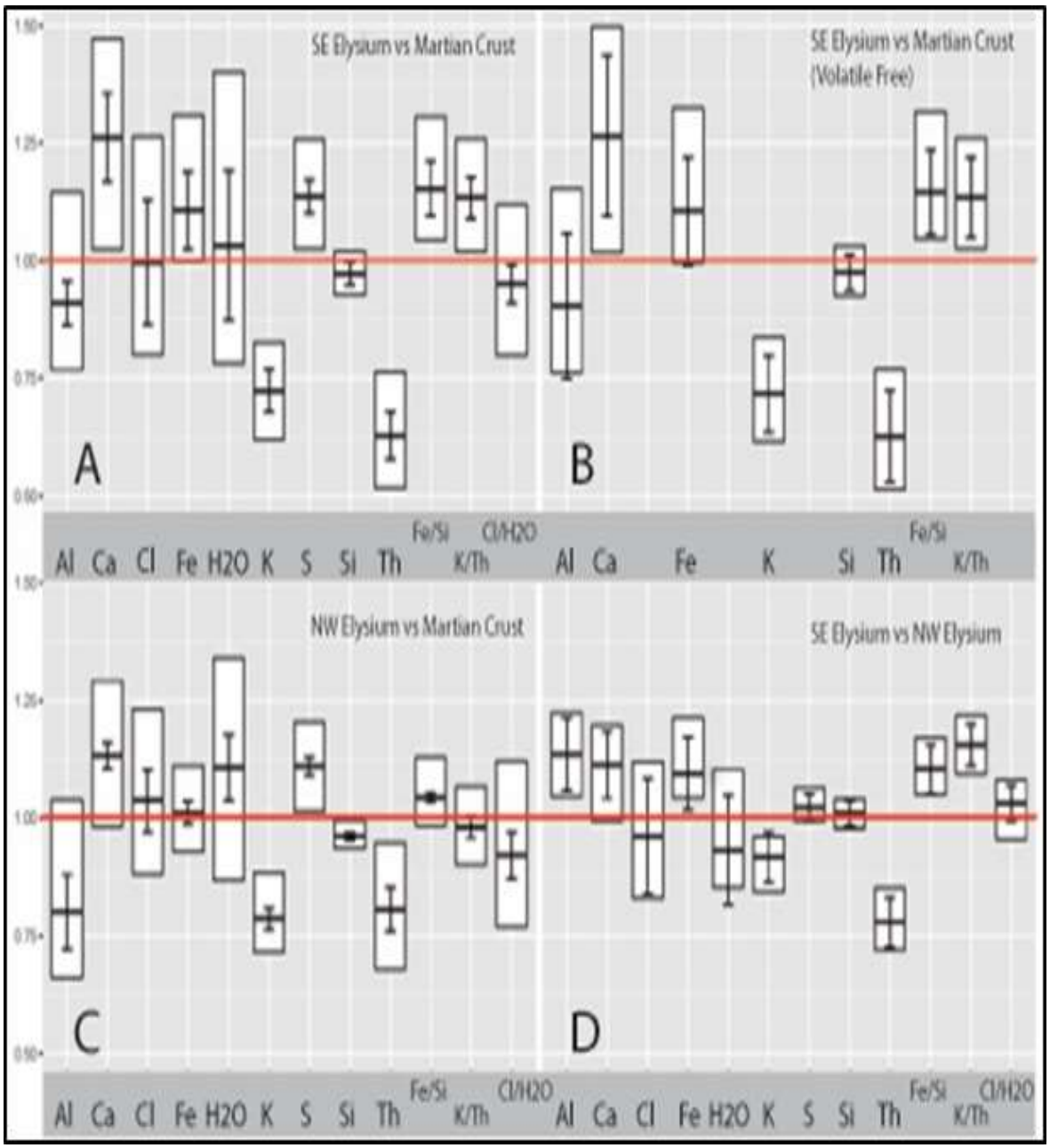

Figure 4. Ratio bound box plots indicate compositional ratios of one target region to another as 75th/25th percentile, 50th/50th percentile, and 25th/75th percentile for the mass fraction of elements and the ratios of Fe/Si, K/Th, and Cl/H2O. Deviation of the median ratio from unity suggests tentative compositional distinctness, while the lack of overlap with unity for a given box shows significant changes, even for small relative differences. Error bars were calculated as the uncertainty of the median average deviations (MAD) using the equation MAD= median [$|X_i$-median (X_i)|], where median (X_i) is the median of all values X_i [Miller and Miller, 2010]. Red lines highlight the 1 to 1 ratio, values below the line represent depletion, while values above represent enrichments. (a) SE Elysium sub-region vs martian crust. (b) SE Elysium vs martian crust, normalized for an observed volatile-free basis, removing Cl, S, and H2O from the bulk composition. (c) NW sub-region vs martian crust. (d) NW Elysium sub-region vs the SE Elysium sub-region.

The γ derived geochemistry is normalized to a volatile and "mobile" element-free basis in order to ensure the compositions investigated in Elysium represent the igneous components at the surface, rather than those affected by interference from the dust. The normalization factors were calculated for each pixel using the standard equation 100/(100-[H_2O]-[SO_3]-[Cl]) [*Taylor et al.*, 2010]. A constant oxidation state of +6 is assumed for S when converting to SO_3 [*Taylor et al.*, 2010]. The results (Figure 4b) reveal that the volatile-free compositions show the same relative trends between the SE and the martian crust as the volatile-bearing compositions, indicating the compositions are cation-conserving [*Hurowitz and McLennan*, 2007], and volatiles merely dilute the abundances of the major elements, rather than dominate a surficial layer.

Compared with the average martian crust, the NW Elysium region has minor enrichments in Ca (1.13±0.03) and H_2O (1.11±0.07), as well as a major depletion in Si (0.96±0.01) and a major enrichment of S (1.11±0.02). The NW region also shows a minor depletion in Al (0.80±0.08) and major depletions in K (0.79±0.02) and Th (0.81±0.05). These results are shown in ratio bound box plot for Figure 4c.

When compared to one another, the two regions of the Elysium Volcanic Province reveal several interesting geochemical trends (Figure 4d). The SE Elysium region displays a minor enrichment of Ca (1.11±0.07) and major enrichments in Al (1.34±0.08) and Fe (1.09±0.08). Both regions have nearly identical abundances of Si (1.02±0.03). Despite both regions having major depletion in the high spectral precision elements, K and Th, relative to the martian crust, the depletion is even more significant in the SE region, which shows a depletion relative to the NW.

This work uses a molar ternary plot [*Nesbitt, H. W. and Wilson*, 1992; *Hurowitz and McLennan*, 2007; *McSween et al.*, 2008; *Ming et al.*, 2008] to further our geochemical analysis of the Elysium provinces and test whether aqueous alteration could explain the observed geochemical

anomalies. This work uses a ternary diagram which has been used to describe the aqueous weathering trends of olivine-bearing basalts, given their pervasiveness in the martian crust, under both moderate pH regimes of typical terrestrial settings [*Nesbitt, H. W. and Wilson*, 1992] and low pH conditions, with low water to rock ratios, where most chemical weathering processes on Mars occur [*Hurowitz and McLennan*, 2007]. The apices of this ternary are (Al_2O_3) – (CaO + Na_2O + K_2O) – (MgO + FeO) [A-CNK-MF] (Figure 5). For the moderate pH conditions on Earth, altered rocks progress from below the feldspar-olivine tie-line, which connects the pure end-member compositions of general feldspar [$(K,Na,Ca)(Al,Si)_2Si_2O_8$] and olivine [$(Mg,Fe)_2SiO_4$], toward the Al_2O_3-FeO+MgO edge [*Nesbitt, H. W. and Wilson*, 1992; *Sigurdur R. Gislason*, 1993]. If done to completion, this alteration would produce clay minerals such as kaolinite [$Al_2Si_2O_5(OH)_4$]. This terrestrial trend is shown by the black "weathering" arrow in Figure 5. The second trend-line corresponds to the results from the alteration of synthetic martian rocks under low pH laboratory conditions, with the altered rock progressing toward to A-CNK edge of the ternary and the alteration fluid progressing toward to MF apex [*Hurowitz and McLennan*, 2007]. Even though the ternary plots have both Na_2O and MgO components, these oxides lack the associated γ-derived chemical data. Consequently, this work uses the method by Baratoux *et al*. [2014] to estimate Na_2O and MgO mole fractions (Methods).

Figure 5 shows the majority of the Elysium chemical provinces' pixels plotting directly on the low pH system aqueous alteration trend line. Pixels from both the NW region (blue) and the SE region (red) overlap and plot near the alteration under low pH trend line (dashed line), close to the unaltered rock composition (white disk), away from the altered composition of basalts (orange disk). The martian meteorites, generally plot below the trend line for low pH aqueous alteration, closer to the CKN-MF edge of the ternary. The APXS-analyzed in-situ rocks from Gusev Crater

generally plot between the low pH aqueous alteration trend line and the Feldspar-Olivine Tie-Line. The unaltered igneous samples plot closer to the martian meteorites, while the altered rocks plot above them, closer to the feldspar-olivine tie-line. The NW and SE Elysium pixels plot on the trend line between the martian meteorites and the unaltered Gusev igneous rock.

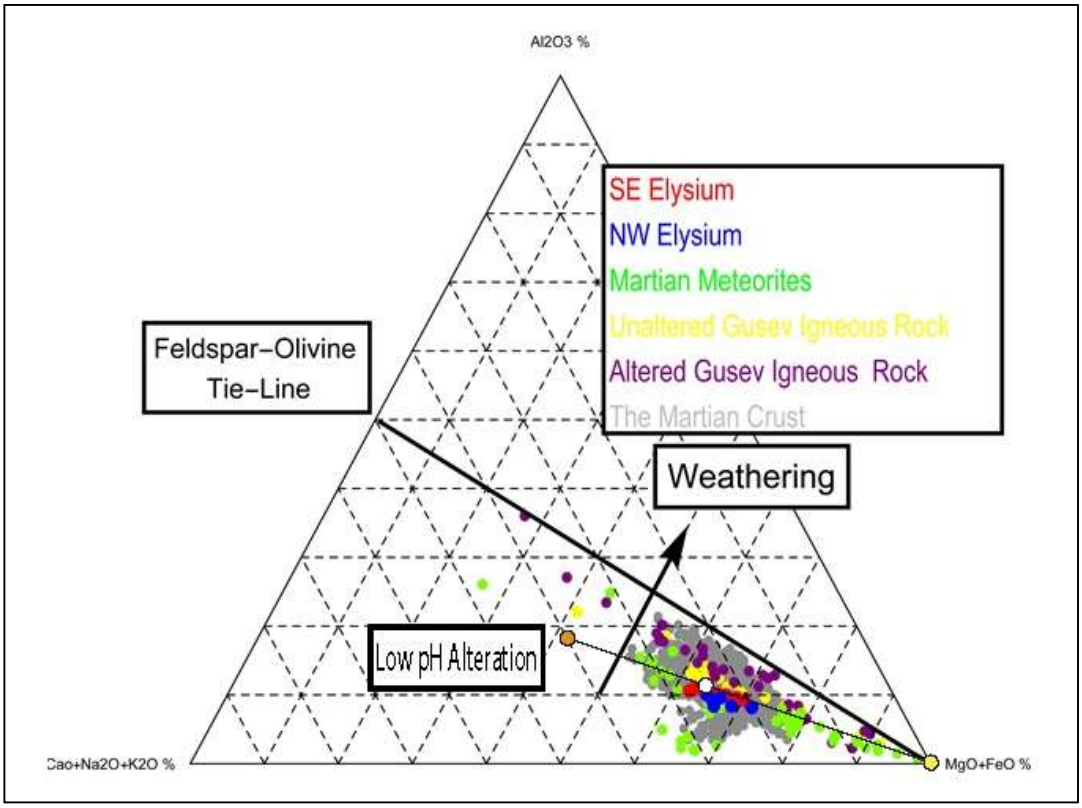

Figure 5. Ternary plot of (Al2O3) – (CaO + Na2O + K2O) – (MgO + FeO) as a proxy for the index of alteration for martian rocks. Open system aqueous alteration trend is shown with the black line, with altered rock (left circle), unaltered rock (middle), and alteration fluid (right). This line corresponds to the results from the alteration of synthetic martian rocks under low pH laboratory conditions by Hurowitz and McLennan [2007]. Plots the pixels from both SE (red) and NW (blue) Elysium vs the martian meteorites (green), unaltered Gusev igneous rock (yellow), altered Gusev igneous rock (purple) and the rest of the GRS data (gray). The data sets form a trend in the direction of more exposure to alteration effects, with the martian meteorites representing compositions of little-to-no alteration, and the altered Gusev samples representing the most heavily altered igneous compositions.

1.4 Discussion and Conclusion

This work identifies a compositional shift temporally and spatially across the Elysium Volcanic Province from the older NW region (3.44 ± .02 Ga) to the more recent SE region (2.59 ±

0.08 Ga). Through the convergence of multiple data sets, this work quantifies the compositional changes in lavas of variable ages across the province. The results indicate that the unique geochemistry of the Elysium Volcanic Province represents igneous processes as opposed to secondary aqueous alteration of the surface or interference from dust.

The resulting 0.85 ± 0.08 Ga difference between the SE and NW Elysium regions estimated by crater counting provides the province with a record of varied magmatic compositions over its geologic history. This in turn, helps to constrain the evolution of Mars as a geologically active planet. The Hesperian/Amazonian temporal boundary is estimated to be between 3.3 to 2.9 Ga, but could also vary as much as from 3.4 to 2.0 Ga due to poorly constrained martian cratering and erosional rates during the time [*Hartmann and Neukum*, 2001]. With this chronology in mind, the SE Elysium region is decidedly Amazonian, while the older NW Elysium province falls at end of the late Hesperian era, just prior to the Hesperian/Amazonian Boundary. Consequently, prior analyses by Baratoux *et al.* [2011], which focused exclusively on the NW region, may not represent the mantle conditions beneath the Elysium Volcanic Province during the Amazonian period as directly as the SE province.

The NW region is depleted in Al, Ca, and Fe compared to the SE region, while K and Th, show significant depletions in the younger flows. In order to compensate for the observed depletions in Al, Ca, and Fe, an unreported major (>10%) rock-forming element must be enriched in the NW to sum the total oxide mass fractions detected by the GRS up to unity for mass balance purposes. The only major rock-forming element not reported by the GRS is Mg, making it a reasonable candidate for the majority of the missing mass fraction. These differences in major element abundances between the two regions have major implications for time dependent changes to the composition of the martian mantle from the late Hesperian to the Amazonian periods.

Elemental ratios can be used to assess the likelihood of secondary geologic processes. Elysium, like much of the northern mid-latitudes, has a surficial layer of fine material dominated by tens of μm micrometer grain size, or "dust" [*Putzig et al.*, 2005; *Jones et al.*, 2014]. This dust is characteristically bright, having high albedo and low thermal inertia, and has been found to partially dominate the geochemical signature of large regions of the planet [*Newsom et al.*, 2007]. Bright dust at the MER rover sites, Gusev and Meridiani, was analyzed using the APXS instrument and found to contain elevated abundances of the more mobile and volatile elements, S and Cl, relative to darker, less mobile soil and rock [*Yen et al.*, 2005]. Evidence of abundant hydrated minerals within the soils was also found using the MER rovers' MiniTES instrument [*McSween et al.*, 2010]. An abundance of dust could cause the elevated levels of S in the SE and both S and H_2O in the NW [*McSween et al.*, 2010; *Karunatillake et al.*, 2014]. If the primary source of volatile elements at Elysium is attributed to a layer of globally-sampled dust deposited by atmospheric processes, then the chemical province should yield a Cl/H_2O ratio similar to the global average. Rather, there is a lower Cl/H_2O ratio in both the SE and NW regions relative to the martian crust (Figure 4a and 4c). More likely, the distinct Cl/H_2O ratio and enrichment in S reflect the volatile content of the magma which formed the Elysium Volcanic Province, as these volatiles are readily sourced from volcanic degassing[*Gaillard et al.*, 2012].

Past work has described dust within the most heavily mantled regions of Mars to be enriched in K and Th rather than depleted [*Newsom et al.*, 2007]. These heavily mantled regions, which include Arabia, Tharsis, and Amazonis, are chemically distinct from one another, indicating that the γ signature is reflective of locally, rather than globally, derived material[*Boynton et al.*, 2007; *Newsom et al.*, 2007]. If this is the case in Elysium, even if the GRS is sampling the signature from the dust, it still reflects the igneous compositions of the region. If the γ signature had been

influenced by the sampling of a thick layer of volatile-enriched dust on top of the bulk basaltic crust, the renormalizing to a volatile-free basis would have caused an apparent enrichment in the remaining elements. The volatile-free ratio bound box plot (Figure 4b) comparing SE Elysium to the martian crust does not reveal any deviation from the relative abundance trends compared to the bulk compositions. This supports the idea that the GRS is primarily sampling the bulk basaltic rock composition.

Effusive lava flows, which result from hot magma outpouring onto the surface, can be greatly influenced by H_2O in its source; even just a few ppm of water in the lava could greatly reduce its viscosity[*Grott et al.*, 2012], and NW Elysium shows a minor enrichment of H_2O in the γ data relative to the martian crust. As mentioned previously in this work, morphologies characteristic of effusive flows such as ropey, lobate textures, sinuous channels, and lava tubes dominate the landscape across both regions of Elysium. The rootless cone structures within SE Elysium could indicate a wet environment with higher than average water-to-rock ratios on the surface during the time of emplacement of these lavas, but they do not appear to be widespread enough to dominate regional geochemistry. In addition to morphology, calculations done by prior work for the temperature of NW Elysium magmas also favor a relatively hot source, with mantle potential temperatures of 1405˚ C, the highest of any Amazonian volcanic province analyzed by that work[*Baratoux et al.*, 2011]. This high temperature would suggest a deep mantle origin, and would agree with the undepleted magma compositions, with high abundances of volatiles, such as H_2O, that are observed in the γ data.

The temporal variation between the two regions is consistent with magmatic variability and provides a degree of insight into the igneous evolution of the Elysium Volcanic Province. The observed geochemical trends suggest a difference in source signature between the older NW region

and younger SE region (Figure 4). Two possible interpretations arise to explain these temporal variations in geochemistry. The first is that of a heterogeneous mantle, with pockets of distinct compositions contributing to the geochemical signatures observes on the surface at different periods in martian history. Multiple models exist to describe how the martian mantle might be compositionally heterogeneous both laterally and vertically. The possibility of a whole-mantle magma ocean on early Mars has been speculated. The model predicts solidification of multiple zones of cumulates in the mantle at different depths, which eventually differentiate into distinct lateral components, when the deeper cumulates rises and settle at neutral buoyant forces nearer to the shallow zone[*Elkins-Tanton et al.*, 2005]. This mantle overturn leads to lateral heterogeneity, with multiple zones of cumulates of different densities, within mantle sources. Differences in mineral content is expected to be observed in the eruptions from these sources, with regions dominated by specific minerals, with lower density cumulates being enriched in MgO and higher density cumulates being enriched in FeO [*Elkins-Tanton et al.*, 2005]. It is worth noting that Fe, which other than Si, is the most abundant element detectable by the GRS and shows significant variability between the two regions. Fe may prove to be a more useful indicator of mantle overturn at regional scales across Mars.

Recent work by Balta & McSween [2013b] has described a separate model for martian mantle evolution which could lead to source heterogeneity. This model proposes that older Hesperian volcanoes were sourced from a portion of the upper depleted mantle, while the younger Amazonian volcanoes were occasionally sourced from upwelling from a deeper undepleted portion of the mantle. This upwelling provides the surface with water-rich, shergottite-like compositions [*Balta and McSween*, 2013b]. These lavas of distinct age and composition within Elysium could potentially represent a regional expression of this global mantle evolution. This is unlikely,

however, because the compositions observed in the two regions of Elysium (i.e. relative enrichment in Fe and H_2O for the younger SE region) do not match expectations of the model by Balta & McSween [2013b], which predicts higher concentrations of Th and H_2O and depletions in Fe for the younger eruptions.

The second interpretation of possible igneous processes exists as a change in depth of the melt formation in the mantle beneath the Elysium Volcanic Province. This is made possible by a model which predicts continual mantle plumes rising to the surface throughout Elysium's lengthy eruptive history during the late Hesperian and Amazonian Eras [*Dohm et al.*, 2008]. The loading of the lithosphere by the formation of the super-shields could cause the lithosphere to flex and increase the pressure on the mantle source over time. This increase in pressure would correspond to an increasing depth of melt formation. The younger volcanism in the SE, where lithospheric thickness is considerably lower [*Baratoux et al.*, 2014], would take place with lower pressures and at shallower depths. With distinct depth to melt formations between the Hesperian and Amazonian, magmas erupted with notably different abundances of elements. This is supported by the compositional distinctness between the NW region and SE region of several major and minor elements (Figure 4d), most notably Th and Fe. The higher concentration of Th in NW Elysium suggests a lower degree of partial melting in the mantle source [*Baratoux et al.*, 2011], while the elevated Fe abundance in the SE is likely indicative of a change to a shallower source depth [*Auzende et al.*, 2008] in SE Elysium.

Based on our results, the geochemistry seems most consistent with a model for the change in the depth of melt formation in the mantle beneath the Elysium Volcanic Province. This conclusion has major implications for the history of martian mantle evolution, such as how volcanic provinces were built up over time, and motivates future investigations into this province.

Petrologic modeling techniques using pMELTS program to model the partial melting of the bulk silicate compositions of Mars proposed by Taylor [2013] might help us to constrain how the compositions of volcanic provinces changes with variable pressures and degrees of partial melting.

Chapter 2: Petrologic Modeling of Magmatic Evolution in The Elysium Volcanic Province

2.1 Introduction

The Elysium Volcanic Province is a massive expanse of land made up of many hundreds of lava flows of various ages [*Hartmann and Berman*, 2000; *Dohm et al.*, 2008; *Vaucher et al.*, 2009; *Jaeger et al.*, 2010; *Tanaka et al.*, 2014a]. The variable surface ages within this volcanic province have distinct elemental compositions based on the derived values from the Gamma-neutron ray spectrometer (GRS) instrument on board the Mars Odyssey Orbiter [*Susko et al.*, 2017]. Without seismic data or exposed ophiolite sequences on Mars, the compositions of lavas on the surface provide some of the only information we have to study the properties of the interior of the planet. The young age of the surface and isolated nature of the Elysium Volcanic Province in the northern lowlands of Mars make it ideal for analyzing the mantle beneath Elysium during the most recent geologic era on Mars.

The MELTS algorithm is one of the most commonly used programs for simulating compositions and mineral phases of basaltic melt crystallization [*Balta and McSween*, 2013a]. The algorithm calculates solid-liquid relations of a crystallizing melt based on thermodynamic properties of each phase and a selected range of temperature and pressure conditions The program calculates solid–solid and solid–liquid equilibria in silicate systems at high temperature and pressure using Gibbs free energy minimization [*El Maarry et al.*, 2009]. It has been used extensively for both terrestrial applications [*Ding and Dasgupta*, 2017] as well as for planetary science models which have been applied to both lunar [*Sakaia et al.*, 2014] and martian settings [*El Maarry et al.*, 2009; *Baratoux et al.*, 2011; *Balta and McSween*, 2013a]. Specifically, the pMELTS calibration of the algorithm allows for higher pressure (10-30 kbars) regimes than the MELTS algorithm provides, and is more appropriate for modeling melt compositions and

equilibrium condition for a source within the martian mantle. The pMELTS version of the program can be used to model how partial melting of the bulk silica compositions for Mars could produce compositions similar to those derived from the GRS data [*El Maarry et al.*, 2009]. Simulations using chemistry from multiple surfaces of variable age within the volcanic province can be used to determine various spatio-temporal dependent conditions which might provide insight into how mantle properties from beneath Elysium have altered over the course of the Amazonian period.

Modeling techniques using pMELTS have been used to estimate the thickness of the lithosphere in the Tharsis Region and the mantle conditions during the time of resurfacing events in the region [*El Maarry et al.*, 2009]. Work by El Maarry [2009] used pMELTS to estimate a pressure of 15-20 kbars and a degree of partial melting of 3-20% for the magma source. On Mars, this corresponds to a depth of melt formation of 125-170 km. The authors found this estimation to be consistent with several other models for the lithospheric thickness and depth of source for the Tharsis region, which predicted a range of 150 km under Olympus Mons [*Thurber and Toksoz*, 1978]. In their work, El Maarry et al. [2009] identified that the pMELTS algorithm is not optimized for Fe-rich parent magmas, such as those within Mars's mantle. The authors note that work carried out by Hirschmann et al. [1998] compared experimental results and identified that the algorithm overestimates the stability of the mineral Orthopyroxene in its calculations. El Maarry et al. [2009] compared their results to values found experimentally [*Bertka and Holloway*, 1994] at 15 kbars (Table 3) and determined that while the trends in oxide compositions of the liquid phase are the same, they differ systematically by a few wt% relative to the experimental values for the oxides SiO_2, FeO, and Al_2O_3. An offset value can be calculated and then be applied to the resulting liquid compositions from pMELTS to correct for an Fe-rich mantle source. Since, the general changes in

trend of the liquid compositions is consistent for each oxide over a pressure range close to 15 kbars (10-30 kbars), this offset can be considered robust for this modeling.

Table 3. The oxide content results of 5 partial melting experiments carried out by Bertka & Holloway [1994]. Experiments used Fe-rich parental magmas compositions, JFR and DW, at 15kbars.

	JFR-4 (10%)	DWF-27 (30%)	error	DWF-73 (32%)	error	DWF-37 (55%)	error	DWF-38 (71%)	error	Average
wt%	10	30		32		55		71		
SiO2	44.9	45.9	0.5	45.9	0.9	47.3	0.5	47.7	1.1	46.37
TiO2	1.49	0.47	0.02	0.45	0.03	0.29	0.02	0.21	0.03	0.40
Al2O3	13	7.49	0.06	7.38	0.26	5.43	0.24	4.18	0.28	6.77
FeO	17.3	19.5	0.5	20.8	0.8	19.8	0.2	17.8	0.3	20.03
MnO	0.38	0.56	0.06	0.58	0.04	0.5	0.03	0.48	0.04	0.55
MgO	8.89	16.2	0.6	15.8	1	20.1	0.8	24.3	1.4	17.37
CaO	9.57	7	0.21	6.54	0.44	4.4	0.23	3.42	0.2	5.98
Na2O	3.82	1.67	0.05	1.37	0.14	1.08	0.05	0.76	0.16	1.37
P2O5	0.54	0.51	0.11	0.56	0.13	0.22	0.11	0.22	0.03	0.43
Cr2O3	0.14	0.63	0.14	0.61	0.1	0.91	0.06	0.88	0.05	0.72
Total	100.03	99.93		99.99		100.03		99.95		99.98

In this chapter, petrologic methods are used to investigate the surface compositions of the lava flows within the Elysium Volcanic Province and to model the martian mantle beneath the province. These models are used to infer the mantle conditions and provide insight into the evolution of lithosphere beneath this region over time. Specifically, this work uses the program pMELTS to model how partial melting of the martian mantle could evolve magmas into the surface compositions derived from the GRS instrument. By performing these simulations with varying initial conditions and comparing the results to geochemistry of the surface of several sub-regions of variable age within the volcanic province, this work models how the mantle beneath Elysium has changed over time and makes predictions for how martian volcanic provinces evolve globally. This work establishes that these changes are likely due to lithospheric loading by long term,

episodic volcanism within the Elysium Volcanic Province over a 3.5 Ga history [*Dohm et al.*, 2008].

2.2 Methods

In this work, the Elysium Volcanic Province is delineated further than in Chapter One. Three sub-regions, based on unique geochemistry and mapped geology, are used to reveal a variable surface age across the province (Figure 6) [*Susko et al.*, 2017]. The first sub-region is the southeast (SE) Elysium sub-region and is the youngest of the three. It has been delineated on the basis of a characteristic depletion in the large-ion-lithophile (LIL), radioactive elements K and Th [*Karunatillake et al.*, 2009], which are the two elements with the strongest coupling effect in igneous settings [*Taylor et al.*, 2006; *Gasnault et al.*, 2010]. This region is also dominated by the Late Amazonian Volcanic Unit in mapped geology. The Central Elysium sub-region has the same characteristic depletions in K and Th, but the mapped geology is dominated by Amazonian-Hesperian Volcanic units [*Karunatillake et al.*, 2009]. The last sub-region is the northwest (NW) Elysium. This is the oldest sub-region, with an age of approximately 3.44 Ga [*Susko et al.*, 2017] with a surface dominated by various Hesperian-aged geologic units [*Tanaka et al.*, 2014a].

This work seeks to advance the analytical method in the work by El Maarry et al. [2009] in several ways when applying the method to the Elysium Volcanic Province. First, where El Maarry et al. [2009] ran pMELTS calculations for only a 3 different, anhydrous pressure conditions (30 kbars, 20 kbars, and 15 kbars), this work runs trials at a range of pressure conditions with a much smaller pressure interval to get the most precise estimates of mantle condition possible. This work also considers magma source region conditions with three different possible H_2O compositions

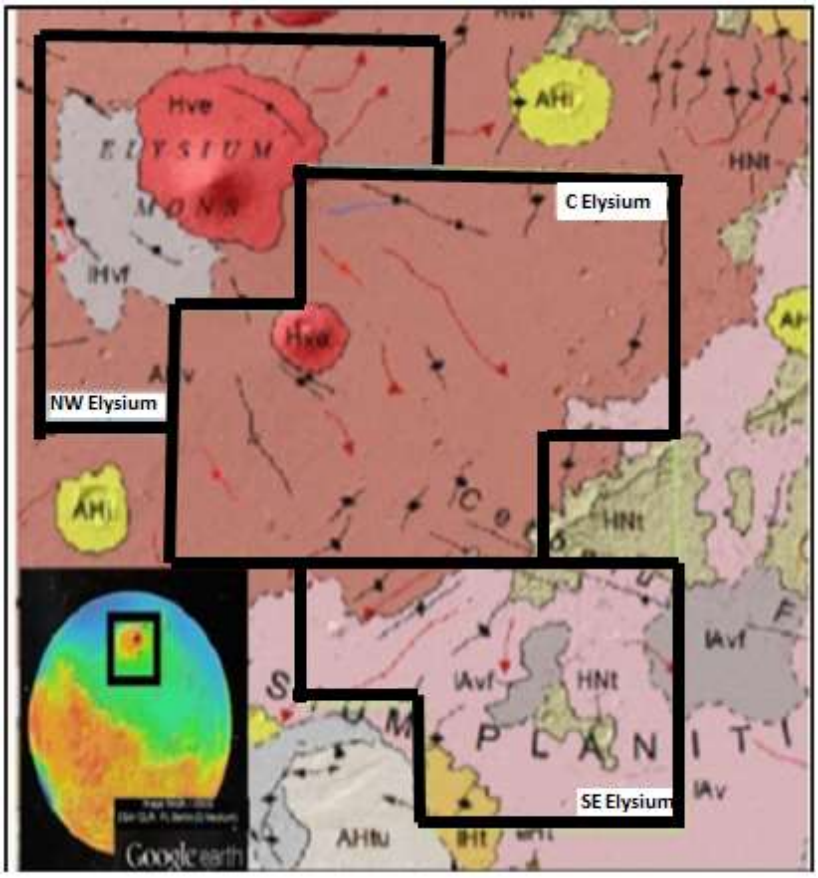

Figure 6. Updated Geologic map of Elysium Volcanic Province from the first chapter. This new map delineates the two sub-regions into three based on mapped geologic units. The Central Elysium unit is dominated by the AHv unit (Amazonian-Hesperian volcanics), while the SE is dominated by the lAvf (Late Amazonian volcanic fields). Geologic map by Tanaka [2014a]. North is up in the map.

estimated by previous work [*Dreibus and Wanke*, 1987; *Leshin*, 2000; *McCubbin et al.*, 2012; *Taylor*, 2013]. By doing this, this work attempts to constrain how sensitive the results from pMELTS are under variable H_2O concentrations. Second, where El Maarry et al. [2009] used the Dreibus and Wanke [1985] (DW85) composition for bulk silicate Mars to approximate the composition of the mantle, this work uses a recently updated bulk silicate Mars composition based on a wider suite of martian meteorites [*Taylor*, 2013]. Last, where El Maarry et al. [2009] looked at the liquid compositions of only 4 oxides (SiO2, FeO, Al2O3, and CaO), this work uses the results from seven oxides (adding K_2O, TiO_2, and MgO to the list), calculating experimental offsets

for all of them, and comparing the results in order to find the source conditions for the lava compositions at the surface in Elysium based on as many oxides as possible.

When entering the model parameters into pMELTS, one of the most important values to consider is the H_2O content of the parent magma. Even a few 10s of ppm H_2O in the melt can greatly depress the solidus and lower the viscosity of the melt [*Grott et al.*, 2012], and can have an effect on the resulting liquid compositions. The water content of the martian mantle during the times of the Elysium Volcanic Province eruptions and subsequent emplacement of lava flows is still highly debated. Dreibus and Wanke [*Dreibus and Wanke*, 1987] provide an estimate of 39 ppm of H_2O. This seems to be an underestimation, based on the evidence of how water has influenced the evolution of the martian crust as well as more recent measurements of water found in hydrated veins of martian meteorites. Leshin et al. [2000] and McCubbin et al. [2012] measured the H_2O composition of apatites found in both a depleted shergottite martian meteorite and an apatite from an enriched martian meteorite shergottite (Shergotty). These values were used to calculate a range of 730-2870 ppm H_2O for the parental magmas which crystallized these meteorites. On the other hand, Taylor [2013] estimated a range of 150-220 ppm H_2O. In this work, the pMELTS program runs for a variety of hydration states to assess the most likely content of the parental magma which produced the compositions observed in the lava flows by the GRS. This work runs simulations using H_2O compositions of 39 ppm [*Dreibus and Wanke*, 1987], 185 ppm [*Taylor*, 2013], and 1800 ppm [*McCubbin et al.*, 2012]. The latter two concentrations represent the median value of the range provided by Taylor [2013] and McCubbin [2012] respectively.

For insight into the igneous rock composition of Elysium's crust, each of the new sub-regions is characterized geochemically and comparisons are made between the three Elysium sub-regions. This analysis includes both bivariate oxide comparisons and a Total Alkali Silica (TAS)

diagram. These are created from GRS data on an anhydrous basis, removing influences from mobile elements: Cl and H2O. This work uses the method by Baratoux *et al*. [2014] to estimate the unreported oxide wt % (MgO, MnO, TiO_2, Na_2O, and P_2O_5) to better characterize the geochemistry of the Elysium Volcanic Province. This work follows the precedent by Baratoux et al. [2014] and neglect the S content of the GRS data (Chapter One). S on Mars is likely constrained to surficial sulfates derived solely from volcanic outgassing and is an insignificant component of the basaltic lavas, furthermore supported by the absence of S found within the martian meteorites. The results of this characterization are listed in Table 4 along with the oxides calculated from Baratoux's method in bold to indicate them as estimations based on ratios from martian meteorites.

Table 4. Summary of geochemical data from the GRS data for the Elysium Volcanic Province. Elemental data has been stoichiometrically converted to their wt% oxide. Values have been normalized to be H2O- and Cl- free. Bolded values are oxides calculated using the ratios and equations defined by Baratoux et al. [2014]. Error bars are calculated as the standard error of the arithmetic mean of all pixels within a sub-region.

	Central	Error	SE	Error	NW	Error
Al2O3	8.08	0.16	8.85	0.52	7.25	0.50
CaO	8.45	0.68	9.79	0.16	8.10	0.44
FeO	18.2	0.83	21.4	0.62	17.2	0.43
K2O	0.31	0.02	0.34	0.01	0.35	0.01
SiO2	42.4	0.96	45.0	0.39	42.9	0.68
Th (ppm)	0.39	0.03	0.43	0.05	0.51	0.02
P2O5	**1.32**	**0.07**	**1.46**	**0.06**	**1.50**	**0.05**
TiO2	**1.52**	**0.08**	**1.68**	**0.07**	**1.72**	**0.06**
Na2O	**2.09**	**0.11**	**2.31**	**0.10**	**2.37**	**0.08**
MnO	**0.45**	**0.02**	**0.53**	**0.02**	**0.43**	**0.01**
MgO	**17.2**	**2.19**	**8.64**	**1.75**	**18.2**	**1.76**
Sum	100.00		100.00		100.00	

For insight into Elysium's igneous crust, we construct a TAS diagram, which plots the total alkali oxide (Na_2O and K_2O) composition on the Y-axis with the total silica compound (SiO_2) on the X-axis. We use the elemental mass fraction from the GRS to generate stoichiometrically

equivalent K_2O, Na_2O, and SiO_2 mass fractions. The location of the data on the plot indicates the general type of extrusive igneous rock, based on the composition of these three oxides. Underlying systematic errors leading to uncertainties in GRS spectral data for Si and K values could shift the distributions both vertically and laterally in the bivariate space, undermining the accuracy of plotted GRS data on the TAS diagram.

Compositional data of 42 unique Martian meteorites collected from NASA's Martian Meteorite Compendium (http://curator.jsc.nasa.gov/antmet/mmc/) (Table 1) were plotted on the TAS diagram after normalizing the wt% elemental values for Si the alkali elements to an anhydrous and Cl-free basis and by calculating their oxide phase stoichiometrically (SiO_2, K_2O, and Na_2O). Since the T13 bulk silicate composition was estimated on the basis of martian meteorite compositions, this work includes the martian meteorites for comparison with both T13 and for general comparison with the SiO2 and Alkali geochemistry of the three Elysium sub-regions derived from the GRS spectra. In addition, the TAS diagram can help to quantitatively identify any overlap between the meteorite chemical signature and the Elysium γ spectra in each sub-region.

Modeling for this work was done using a parental melt composition calculated by Taylor [2013] which simulates the bulk silicate Mars composition (T13). The volume of the martian crust is insignificant relative to the volume of the martian mantle, and the crystallization of the crust from an early magma ocean [*Elkins-Tanton et al.*, 2005] is unlikely to greatly affect the bulk silicate composition. For this reason, this T13 composition for bulk silicate Mars can be considered an appropriate proxy for the composition of the martian mantle. This composition (Table 5) was calculated based on the compositions of martian meteorites, with the assumption that refractory element compositions were similar to the values of chondritic meteorites. This was a similar

method to the work by Dreibus and Wanke [1985], which calculated a parental melt composition used in several attempts to model the partial melting of the martian mantle using pMELTS [*El Maarry et al.*, 2009; *Baratoux et al.*, 2011, 2013; *Balta and McSween*, 2013a]. The major difference was that Taylor [2013] incorporated the chemical compositions from more than twice the number of martian meteorites used by Dreibus and Wanke [1985]. Both the DW85 composition and the T13 compositions indicate that Mars mantle is significantly more Fe-rich than Earth's mantle and that it contains a higher proportion of orthopyroxene relative to the amount of olivine.

Since melt formation has to occur beneath the elastic portion of the lithosphere of Mars, this work uses a range of initial pressure conditions which correspond to possible thicknesses of the martian lithosphere [*McGovern et al.*, 2002; *Belleguic et al.*, 2005; *Baratoux et al.*, 2011]. For the pMELTS simulations, this work selected a pressure range of 10-30 kbars with steps of 2 kbars, for a total of 11 unique pressure conditions. This work also runs the program a 12^{th} time at 15 kbars in order to calculate an oxide offset, using the same method as El Maarry et al. [2009]. This work selected a very wide range of temperatures from 2000˚C down to 1000˚C in increments of 10˚C in order to be sure to encapsulate compositions that would extend from above the liquidus to below the solidus for any given pressure conditions. The small temperature increments provide results with enough resolution to select liquid compositions as a function of partial melting at melt fractions of 3%, 5%, 10%, 20%, 30%, 40%, and 50%. These intervals allow me to plot oxide compositions in terms of partial melting for each pressure and H_2O content. Each of these temperature-pressure regimes were repeated three times with a different H_2O value estimated by previous work for the martian mantle (39 ppm, 185 ppm, 1800 ppm). Another critical input for the pMELTS program is the reaction pathway for the oxygen buffer. Generally, the oxygen buffer is

Table 5. The bulk silicate composition of Mars, defined by Taylor [2013]. In this work, it is referred to as "T13" and is considered an updated version to the DW85 composition defined in Dreibus & Wanke [1985]. Oxide equivalents are calculated for the major rock forming elements and included as the first 11 entries in the table. This composition was used as the parental magma composition for the pMELTS thermodynamic calculator.

	Taylor (2013)	Error		Taylor (2013)	Error
SiO2	43.7	1	Y (ppm)	2.89	0.52
TiO2	0.14	0.01	Zr (ppm)	7.49	0.6
Al2O3	3.04	0.1	Nb (ppb)	501	0.07
Cr2O3	0.73	0.04	Ru (ppb)	2.6	0.9
FeO	18.1	1	Pd (ppb)	2.4	0.8
MnO	0.44	0.06	Ag (ppb)	4.2	2.8
MgO	30.5	0.05	Cd (ppb)	9.6	6.1
CaO	2.43	0.01	In (ppb)	6.9	2.2
Na2O	0.53	0.1	Sn (ppb)	38.5	7
K2O	0.04	0.002	I (ppb)	36	22
P2O3	0.15	0.047	Cs (ppb)	95	37
Li (ppm)	3	1.7	Ba (ppm)	4.37	0.21
Be (ppm)	47.7	0.4	La (ppb)	439	48
F (ppm)	21	13	Ce (ppb)	1170	110
Na (%)	0.4	0.08	Pr (ppb)	176	5.8
Mg (%)	18.5	0.7	Nd (ppb)	864	60
Al (%)	1.64	0.04	Sm (ppb)	274	13
Si (%)	20.5	0.9	Eu (ppb)	103	6
P (ppm)	675	215	Gd (ppb)	374	31
Cl (ppm)	32	9	Tb (ppb)	67.3	13.2
K (ppm)	309	36	Dy (ppb)	450	17
Ca (%)	1.74	0.04	Ho (ppb)	106	6
Sc (ppm)	11	0.4	Er (ppb)	306	37
Ti (ppm)	832	30	Tm (ppb)	44.8	6.2
Cr (ppm)	4990	420	Yb (ppb)	308	26
Mn (%)	0.34	0.05	Lu (ppb)	44.8	1.7
Fe (%)	14.1	0.8	Hf (ppb)	217	14
Co (ppm)	71	25	Ta (ppb)	27.2	1
Ni (ppm)	330	109	W (ppb)	74	31
Cu (ppm)	2	0.7	Re (ppb)	0.88	0.66
Zn (ppm)	18.9	2.9	Os (ppb)	2	0.8
Ga (ppm)	6.6	0.8	Ir (ppb)	2	1
As (ppb)	86	55	Pt (ppb)	3.1	0.8
Se (ppb)	85	36	Tl (ppb)	1.28	0.71
Br (ppb)	191	58	Bi (ppb)	0.6	0.41
Rb (ppm)	1.3	0.14	Th (ppb)	58	12
Sr (ppm)	14.6	0.7	U (ppb)	16	3

the specific assemblage of minerals that constrain the fugacity of oxygen as a function of temperature. Different pathways are used for rocks with different assemblages of minerals containing elements of various oxidation states. The compositions within The Elysium Volcanic Province are basaltic, which is generally consistent with the results of the TAS diagram. This work uses the oxygen fugacity pathway 3 log units beneath the quartz-fayalite-magnetite buffer (QFM-3), and assumes compositions contain this buffer assemblage. QFM-3 was found to be optimal for martian basalts [*Ghosal et al.*, 1998], and in the work by El Maarry et al. [2009], this pathway was used to successfully estimate the thickness of the lithosphere in the Tharsis region predicted by previous work. This method of handling the thermodynamic calculations led to a total of 36 trials with unique initial conditions for the pMELTS calculator.

In order to calculate an appropriate offset value to correct for the pMELTS simulations, the results from the 15 kbar trials were compared to the experimental results by Bertka & Holloway [1994] and an offset was found and compared to those by El Maarry et al. [2009]. As long as the pressures range used in pMELTS is close to the 15 kbars used in the experimental investigations by Bertka and Holloway [1994], the correction should be effective[*El Maarry et al.*, 2009]. The offsets were calculated by averaging together the difference between the pMELTS results and the experimental values for each wt % oxides at 30%, 32%, and 55% partial melting. The offsets for both the low H_2O content and the high H_2O content (1800 ppm) are listed in the results section. The calculated offset is then applied to the wt% oxide values from the pMELTS output in order to properly analyze the oxide compositions of the surface lavas. Results are compared across a suite of oxides.

In this work, there are similar systematic differences from the experimental values in both this data and the values which El Maarry et al. [2009] reported. Separate offsets are calculated for

the 39 ppm/185 ppm H_2O pMELTS simulations and the 1800 ppm H_2O trials and report each of the offsets to be used in the correction of the pMELTS oxide results. The constant offsets are effective for correcting the systematic differences for the oxides SiO_2, FeO, Al_2O_3, and MgO. The difference between the thermodynamically calculated results and the experimental values varies at a consistent level for these oxides as a function of degree of partial melting. The oxides for TiO2 and CaO, however, still show significant disparity after the offset has been applied. From here, this work uses Mathematica to interpolate both the experimental results as well as the offset between the calculated and experimental results, across the entire interval of 3-50% partial melting. This provided a unique offset for TiO_2 and CaO at each of the percent partial melting, that when applied, align our pMELTS calculations exactly to Bertka and Holloway [1994]'s results at 15 kbars. This method is inadequate for calculating individual offsets of the other 4 oxides at specific percent partial melting. This is because the results by Bertka and Holloway [1994] have a limited number of experimental results with only a few values of percent of partial melting values (10%, 30%, 32%, 55%, and 70% melt). The behavior of the trends between these degrees of partial melting is unconstrained by these experiments, and interpolating a linear trend between these points of % melt causes the trend of these oxides to become suppressed as they are corrected to a linear trend of experimental results.

After using pMELTS to find the pressure and degree of partial melting for compositions most consistent with surface compositions derived from the GRS instrument, the depth at which the melt formed within the martian mantle is calculated using the pressure conditions for each sub-region, the gravitational constant for Mars (3.711 m/s^2), and the average density of martian crust. Recent work which mapped the crustal density of Mars found the Elysium Volcanic Province to have some the highest densities on Mars, in excess of 3300 km/m^3 [*Baratoux et al.*, 2014]. This

value had been calculated independently by other work as well [*McGovern et al.*, 2002]. Belleguic et al. [2005] calculated a density of 3270±150 kg/m^3. A density of 3300 kg/m^3 was used for this work. This is consistent with the expectation for martian basalts containing higher concentrations of Fe and Mg and less Si than terrestrial basalts, and subsequently, having a higher density. The equilibrium temperature of the source, the degree of partial melting, and an adiabatic gradient calculated for the martian mantle, were then used to calculate the mantle potential temperatures for each sub-region. The mantle potential temperature, or the temperature that the solid mantle would have if brought to the surface without an energy exchange with the surrounding rock, effectively corrects the equilibrium temperature to a surface pressure of ~0 bars [*Mckenzie and Bickle*, 1988; *Baratoux et al.*, 2011; *Filiberto and Dasgupta*, 2015]. To calculate the potential temperature of Martian mantle, the average equilibrium temperature had to be corrected to surface pressure conditions (~0 bars) by subtracting the effects of an adiabatic gradient of 0.18°C/km [*Filiberto and Dasgupta*, 2015] and adding the latent heat of fusion for the melt. The latent heat of fusion (T_{fus}) was calculated using the expression $\Delta T_{fus}=F*(H_{fus}/C_P)$, where F is the degree of partial melting, H_{fus} is the heat of fusion of the mantle (6.4× 105 $J*K^{-1}*kg^{-1}$) [*Kiefer*, 2003], and C_P is the heat capacity at a constant pressure (1200 $J*K^{-1}*kg^{-1}$)[*Kiefer*, 2003; *Filiberto and Dasgupta*, 2015].

Each of the Elysium sub-regions are plotted on a figure of depth of partial melting vs mantle potential temperature. Crustal heat flow contours are calculated from depth of melting and mantle potential temperatures using a crustal thermal conductivity of 3.0 $W*m^{-1}*K^{-1}$ [*Baratoux et al.*, 2011]. In this calculation, the mantle potential temperatures are converted to kelvin, multiplied by the thermal conductivity, and then divided by the depth of melt formation. These contours are then

plotted on Figure 12 in terms of depth and mantle potential temperature in order to determine the crustal heat flux throughout the history of the Elysium Volcanic Province.

In order to better understand the crust-mantle system of the Elysium Volcanic Province, a map of crustal thickness for Mars [*Genova et al.*, 2016] is used to calculate the thickness of the crust within each of the sub-regions. This map was generated using gravity and topography data from the Mars Global Surveyor (MGS), Mars Odyssey Orbiter, and the Mars Reconnaissance Orbiter (MRO) to produce measurements of crustal thickness at an extremely fine spatial resolution (<1˚x1˚). Pixels were filtered by the latitude and longitude bounds for each sub-region. The arithmetic mean was then found for all of the pixels within each of the sub-regions.

2.3 Results

Figure 7 shows the GRS pixels for each of the three sub-regions of the Elysium Volcanic Province plotted for three different bivariate comparisons. The NW Elysium region contains 6 GRS pixels, the Central region contains 10 pixels, and the SE region includes 5. In each of the three plots, the pixels for each sub-region cluster together. In Figure 7A, the values for the oxides FeO and MgO were compared to one another because these are the major igneous rock forming oxides and can be indicative of magma conditions at the time of eruption. They have been normalized to SiO_2, the most abundant oxide which also displays the least amount of variance in wt %. The SE Elysium sub-region displays FeO concentrations higher than the other two regions, but contains lower values of MgO. The Central Elysium Sub-region includes moderate values, with higher concentrations of MgO than the SE, but comparable to the values found in the NW Sub-region. It also generally has higher FeO concentrations than the NW, but lower than the SE. It is important to note, that the MgO shown in this figure is the only oxide not directly derived from the GRS data, but rather estimated using the equation by Baratoux et al. [2014].

In Figure 7B, the oxides Al_2O_3 and CaO are compared for the three sub-regions, and all values are normalized to SiO_2. These minor rock-forming elements are useful for comparing to one another because they can give insight into possible mineralogy, such as the types of pyroxenes which have crystallized in volcanic settings. Previous studies have predicted high-Ca pyroxenes, such as potentially augite, in the younger volcanic regions of Mars due to mantle cooling [*Balta and McSween*, 2013b; *Baratoux et al.*, 2013]. Regions partially overlap compositionally relative to their uncertainties for each pixel, but some trends are still visible in the geochemistry. Even though there is some overlap, the consistent spatial trend of increasing CaO from the older NW to the younger SE region increases confidence that it is real. The SE Elysium sub-region generally displays slightly higher CaO than the other two sub-regions, though they can be considered similar to the higher values found within the Central Elysium Sub-region. Likewise, the NW sub-region contains the lowest values for CaO, and can be considered similar to the lower values found within the Central Elysium Sub-region. Both the Central and SE sub-regions contain similar concentrations of Al_2O_3, while the NW contains the lowest concentrations in the province.

In Figure 7C, the oxides of the trace elements K and Th were first converted stoichiometrically to their oxide wt % equivalent, and then K_2O and Th are compared to one another. As in the previous two figures, these oxides have been normalized to SiO_2. K and Th are both large-ion-lithophiles (LILs), naturally radioactive, and incompatible elements with a tendency to concentrate in the melt phase of the magma [*Taylor et al.*, 2006]. This leads them to become depleted from source regions preferentially relative to other elements. Furthermore, K and Th are characterized by a strong mutual affinity during igneous processes. This is apparent in Figure 7C, as the abundances of K_2O and ThO relative to SiO_2 in all three regions positively correlate with

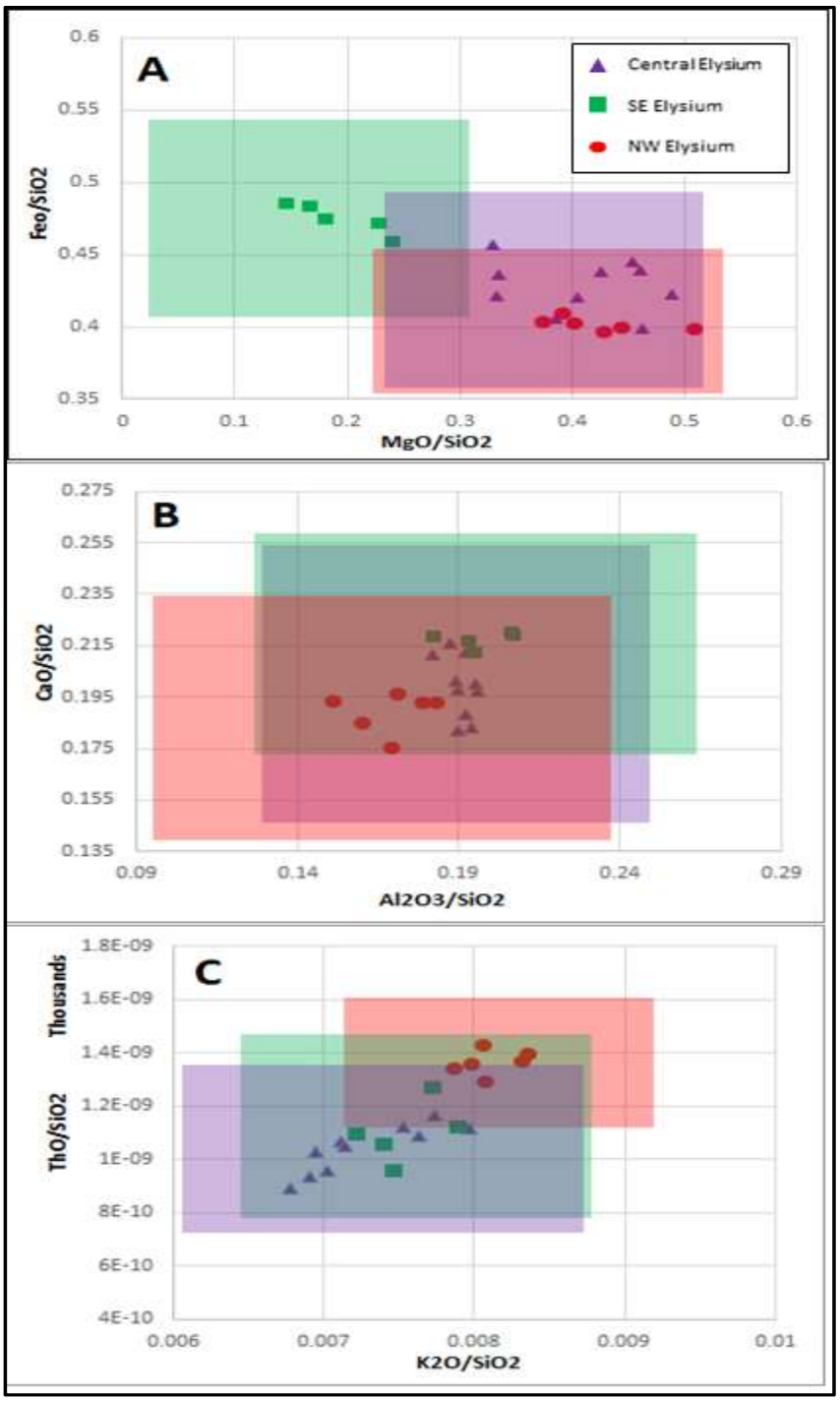

Figure 7. Geochemical data from the GRS for the sub-regions of the Elysium Volcanic Province plotted in bivariate space in order to constrain the chemical uniqueness between sub-regions. SE Elysium (green squares), Central Elysium (purple triangles), and NW Elysium (red circles) are included in all three plots. (A) The major rock forming oxides FeO and MgO both normalized to SiO_2. (B) The minor rock forming oxides Al_2O_3 and CaO, normalized to SiO_2. (C) Comparison of the trace oxides K_2O and Th normalized to SiO_2. Shaded regions represent the extent of the error bars (standard error calculated for each individual pixel) for each oxide for each region.

one another. Generally, the NW Sub-region contains the highest concentrations of both oxides, and the Central Sub-region contains the least, though there is some significant overlap between the concentrations of the SE and Central sub-regions.

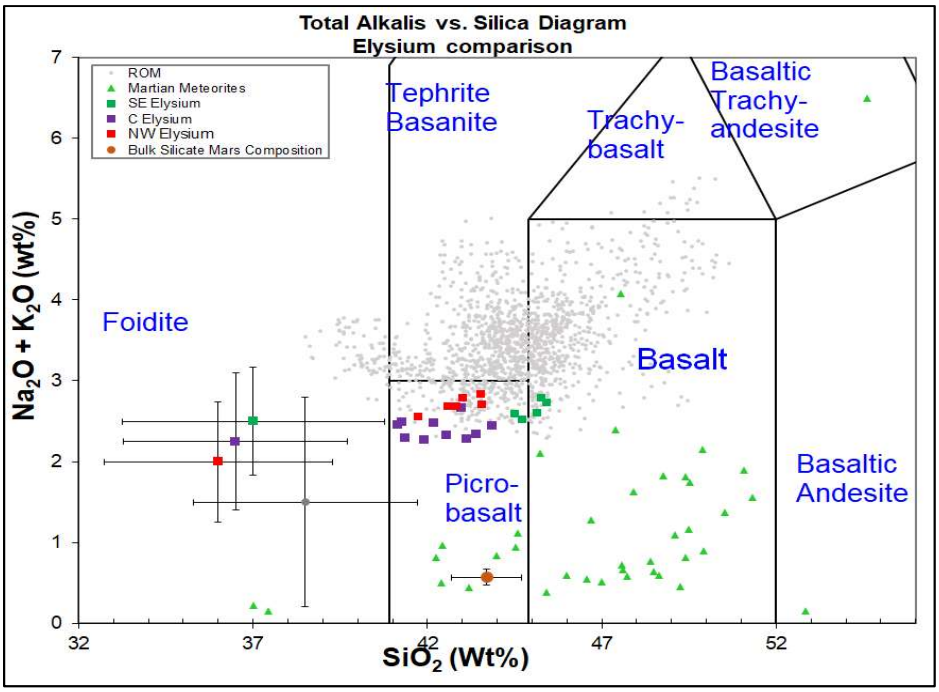

Figure 8. Total Alkali Silica diagram. Data is normalized to an anhydrous composition. Plotting on this figure are the oxide abundances for GRS values for the average martian crust (grey), the NW Elysium region (red), the Central Elysium Region (yellow), the SE Elysium Region (Purple), 42 of the martian meteorites (green), and the bulk silicate Mars composition by Taylor et al 2013 (brown, termed T13 for brevity). TAS diagrams are commonly used to identify types of extrusive igneous rock. Error bars for martian crust and each of the three sub-regions are calculated for a dummy value using the root-mean-square value for uncertainty.

GRS data are mostly concentrated within the basalt or picrobasalt regions on the total alkali-silica diagram (Figure 8) as expected [*McSween et al.*, 2009; *Taylor*, 2013]. The TAS diagram reliably shows relative variations, but provides unreliable constraints on absolute values, due to the Na_2O values estimates using the method by Baratoux et al. [2014] and the manner that the S content of the rock is calculated (described in Chapter One). The possibility of systematic differences between in-situ and remote compositions [*Karunatillake et al.*, 2007] necessitate the normalization of GRS derived compositions to known Si compositions at landing site [*Boynton et al.*, 2007]. This reinforces the usefulness of the GRS data in relative comparisons and analysis,

while the TAS is designed for igneous rock classification based on absolute values [*McSween et al.*, 2009]. Nevertheless, the Elysium data plots between the basalt and the picrobasalt fields. Picrobasalt is a high-MgO variety of basalt, with enriched concentrations of MgO and between 20 - 50% olivine phenocrysts by volume. Whether picrobasalt dominate or not, the TAS diagram shows that the pixels from the Elysium Volcanic Province contain some of the lowest Alkali concentrations relative to the GRS pixels for the rest of the mid-latitudes of Mars. This is still significantly higher than the Alkali composition of the vast majority of the martian meteorites and the T13 bulk silicate composition. They contain roughly average SiO2 values when compared to the rest of the martian crust and overlap with the T13 SiO_2 concentrations.

The pMELTS program is optimized for terrestrial mantle parent compositions, though recently, it has been used extensively to model the partial melting of Fe-rich parent compositions such as DW85 [*El Maarry et al.*, 2009; *Baratoux et al.*, 2011; *Balta and McSween*, 2013a]. The thermodynamic calculations from pMELTS have the same general trends in oxide concentration as a function of melt fraction, but with a systematic difference, offset relative to the experimental values. Hirschmann et al. [1998] attributed this offset to an over stability in the algorithm of the mineral orthopyroxene in the solid phase assemblage of the mantle. This work advances the method used by El Maarry et al. [2009] to correct for the observed offset in the pMELTS calculations. El Maarry et al. [2009] calculated the average offset of the experimental values for 30%, 32%, and 55% partial melting for the 4 oxides SiO_2, FeO, CaO, and Al_2O_3 at 15 kbars. They found values of +2.91 wt% SiO2, -2.94 wt% FeO, and +0.84 wt.% CaO. These offsets were then applied to all subsequent pMELTS calculations. I used the same method to calculate offsets in this study for the oxides: SiO_2, TiO_2, Al_2O_3, FeO, MgO, CaO. The offsets for both the low H_2O content

and the high H_2O content (1800 ppm) are listed in Table 6, while the stepwise offsets calculated for the two oxides TiO2 and CaO are listed in Table 7.

Table 6. Offsets for pMELTS results for the liquid melt oxide concentration. These offset values were calculated in the same manner as those calculated by El Maarry et al. [2009], using the arithmetic means for the difference between pMELTS calculated values at 15 kbar with experimental results by Bertka & Holloway [1994] at 15 kbars for the trials at 30%, 32%, and 55% partial melting. The offsets for SiO2, FeO, and CaO are of the same sign and similar value to the offsets calculated by El Maarry et al. [2009].

	39/185 ppm	1800 ppm
SiO2	2.81	2.22
TiO2*	0.05	0.05
Al2O3	0.04	-0.10
FeO	-2.15	-1.64
MgO	-1.24	-0.54
CaO*	0.74	0.66

Table 7. Interpolated offset values for 3, 5, 10, 20, 30, 40 and 50% melt for TiO2 and CaO. These oxides do not have systematic offsets and instead a stepwise offset is calculated for the degrees of partial melting of interest.

	TiO2			CaO		
% Melt	39 ppm	185 ppm	1800 ppm	39 ppm	185 ppm	1800 ppm
3	1.35	1.40	1.54	2.19	2.06	2.06
5	1.13	1.16	1.28	2.40	2.29	2.29
10	0.69	0.70	0.76	2.63	2.56	2.56
20	0.19	0.18	0.18	2.15	2.13	2.13
30	0.05	0.05	0.05	1.04	1.03	1.03
40	0.05	0.06	0.06	0.31	0.30	0.30
50	0.04	0.05	0.05	0.30	0.30	0.30

For Figure 9, the oxide concentrations in terms of partial melting for SiO_2, FeO, CaO, and Al_2O_3 are plotted in the same manner as El Maarry et al (2009), however this work also include plots for the oxides TiO_2 and MgO, which can be informative for igneous processes. This work

plots the pMELTS outputs for 3 different concentrations of H2O: 39 ppm, 185 ppm, and 1800 ppm. The simulations completed at low H_2O content (39 ppm and 185 ppm) are nearly indistinguishable from one another for every oxide and the same offset is used for both trials. Both these trials are shown with a blue trend line in Figure 9. SiO_2 concentration in the liquid initially increases as a function of partial melting, but begins to decrease at roughly 5% melt, before starting to increase again at ~18%. The trend again reverses at ~65% melt. FeO also starts with increase in concentration as a function of partial melting. FeO in the liquid levels out at ~30% melt and begins to decrease at ~40% melt fraction. These two oxides contained the largest offset in the work by El Maarry et al. (2009). TiO_2 begins with an increasing trend, but begins to decrease exponentially between 3 and 5% partial melting. MgO shows a constant increase as partial melting increase, while Al_2O_3 shows a constant decrease across the entire interval. Last, CaO shows an increase with partial melting until the 18-20% interval, when it starts a steady decrease.

The results from Figure 10 reveal how the oxide composition of the liquid component vary with pressure, degree of partial melting, and H_2O concentration. The mass fraction of each oxide: TiO_2, Al_2O_3, FeO, MgO, CaO, and K_2O is compared with that of SiO_2 in terms of degree of partial melting and pressure. Each plot includes 11 melt curves which show the composition of oxides as a function of degree of partial melting from 3-50%. Each curve corresponds to a pMELTS trial with a unique initial pressure condition ranging from 10 kbars to 30 kbars with an interval of 2 kbars. All of these melt curves together form a pressure continuum, which are used to determine mantle pressures at the melt source for the Elysium Volcanic Province. The SiO_2 content of the liquid generally decreases with increasing pressure conditions. In every plot of Figure 10 the 10 kbar melt curve is located on the far right of the plot and progresses to the left with increasing pressure until 30 kbars, which is located on the far left. For every trial with the same oxide

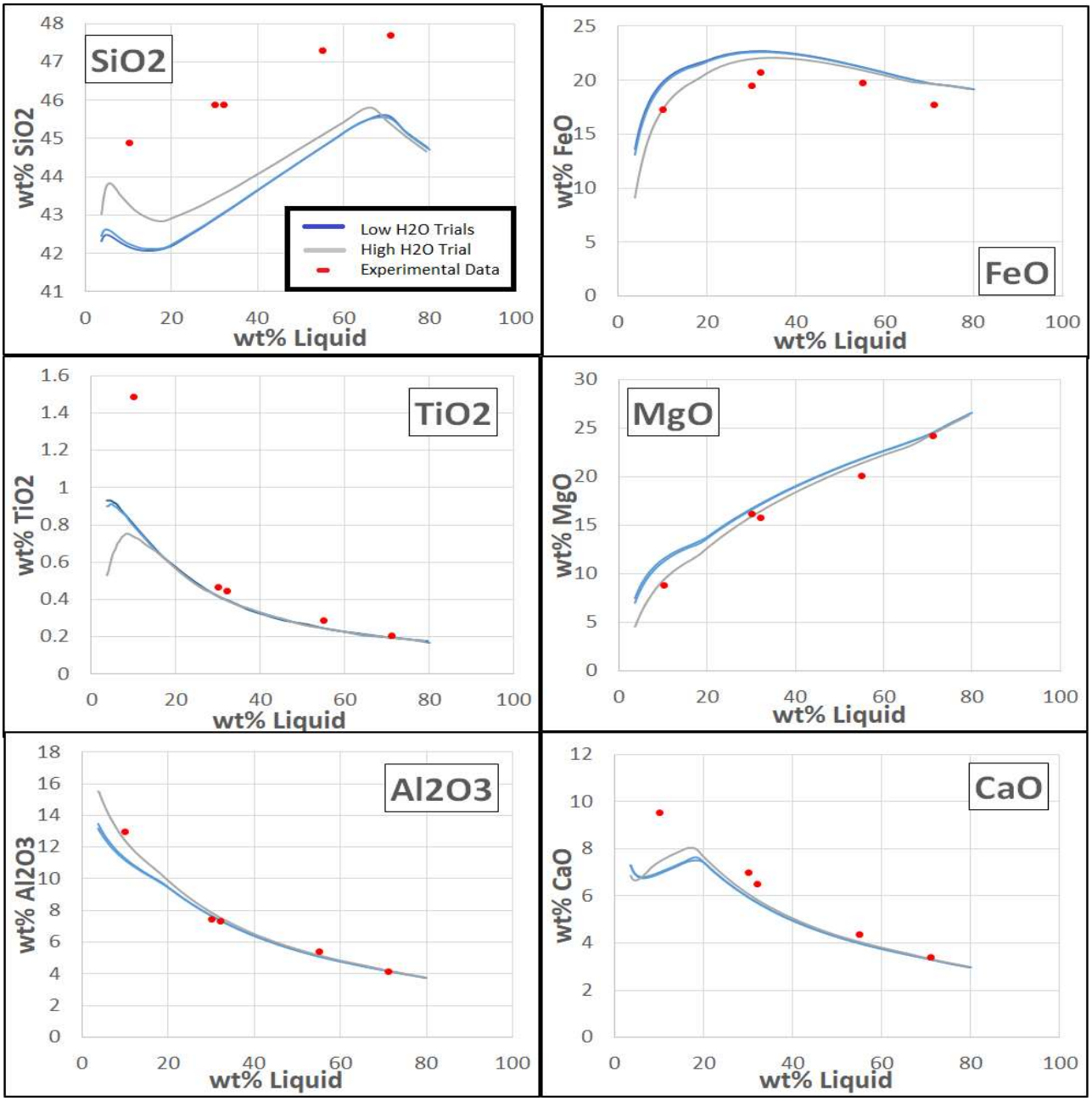

Figure 9. A comparison of the results from pMELTS for six oxides with the experimental values from Bertka & Holloway (1994) (Table 3) at 15 kbars. Each line represents a series of compositions produced by the results from pMELTS for each pressure and temperature combination. Data points are connected with a solid line. The blue lines represent the trend in oxide results from pMELTS trials with H_2O concentrations of 39 ppm and 185 ppm, while the grey lines represent the trend for the trials with an H_2O concentration of 1800 ppm. These plots are useful in displaying the trends of the major oxides in terms of the percent melt fraction according to the thermodynamic calculations by pMELTS. The oxide trends are compared to the experimental results for iron-rich parent compositions at 10, 30, 32, 55, and 71 percent melt fraction (red circles) in order to identify systematic differences of PMELTS from laboratory conditions. The resulting offsets allow for the comparison of the liquid oxide compositions from pMELTS with the oxide concentrations derived from the GRS data for the surface within The Elysium Volcanic Province.

combination, the direction of the composition trend in terms of partial melting stays the same, though as pressure increases the variations in the trend become more subdued and the path becomes more linear.

The average GRS derived values for each of the three Elysium sub-regions have also been included on each plot. Their location relative to the pressure trial curves is used to determine a possible range of pressures and degrees of partial melting for the magma source beneath the Elysium Volcanic Province. Rather than using the uncertainty of the GRS measurements, which is especially complicated for GRS-based analyses due to the biasing effect of spatial autocorrelation [*Karunatillake et al.*, 2011], error bars for each of the sub-regions were calculated using the standard error of the mean using the equation: $s_m=s/N^{1/2}$. Where "s" is the standard deviation.

The offset corrections have been applied to all of the results from pMELTS, except for K_2O, which was the only oxide used in this figure that did not have a corresponding reported value in the experimental work by Bertka and Holloway [1994]. Nevertheless, K_2O displays a low level of variation between GRS pixels relative to other oxides and the locations of the Elysium pixels on the SiO_2-K_2O continuum compare favorably for pressure and degree of partial melting to the other SiO_2-oxide pressure continuum.

The results from Figure 10 are consistent with the liquid SiO_2 composition decreasing with increasing pressure. This is also the case for the oxide Al_2O_3, while FeO and MgO tend to increase. TiO_2, CaO, and K_2O show more complicated variation that is more dependent on degree of partial melting than pressure.

The results of Figure 10 also show that H_2Ocontent of the parental magma does not greatly affect the liquid composition trend, especially at the two lower concentrations 39 ppm and 185 ppm, which are nearly indistinguishable in both Figures 9 and 10. For this reason, the pMELTS calculated liquid compositions for the trials containing 39 ppm (solid line) and 185 ppm (dashed line) H_2O have been plotted together on the same figure (Figure 10A). The trials containing 1800 ppm H_2O show some slight variation when compared to the first two concentrations, and have been plotted in a separate figure (Figure 10B) for the purposes of clarity. These variations between the 39ppm/185ppm runs and the 1800ppm do not add significant variability to the resulting pressures approximated for the Elysium sub-regions. The largest variation between the pMELTS simulations of variable H_2O concentration is in the degree of partial melting. The difference in partial melting between H_2O concentrations is smaller for a particular oxide pair, in many cases, than the difference between degree of partial melting approximations estimated for separate oxide pairs under the same H2O concentrations.

For every plot in Figure 10, the SE Elysium sub-region consistently shows the lowest pressure conditions for equilibrium in the magma source. The NW and the Central sub-regions show much more comparable pressures, but the Central tends to be slightly higher across the oxide pairs. A visual approximation places the SE data points in between the 14 kbar and 16 kbar melt curve for nearly every oxide. The one exception is FeO, which places the average composition directly on the 16 kbar melt curve for both Figures 10A and 10B. The NW and Central sub-regions show slightly more variation, but most of the oxides show them plotting between the 18 kbar and 20 kbar melt curves with variations as high as 21 kbars and as low as 17 kbars. For the oxides TiO_2, FeO, and K_2O the average values for the NW sub-region plots to the right of the 18 kbar melt curve for low H_2O concentrations (39 ppm and 185 ppm). The MgO plot for low H_2O

concentration shows the greatest anomaly, with both the NW and Central sub-regions plotting between the 20 kbar and 22 kbar melt curves.

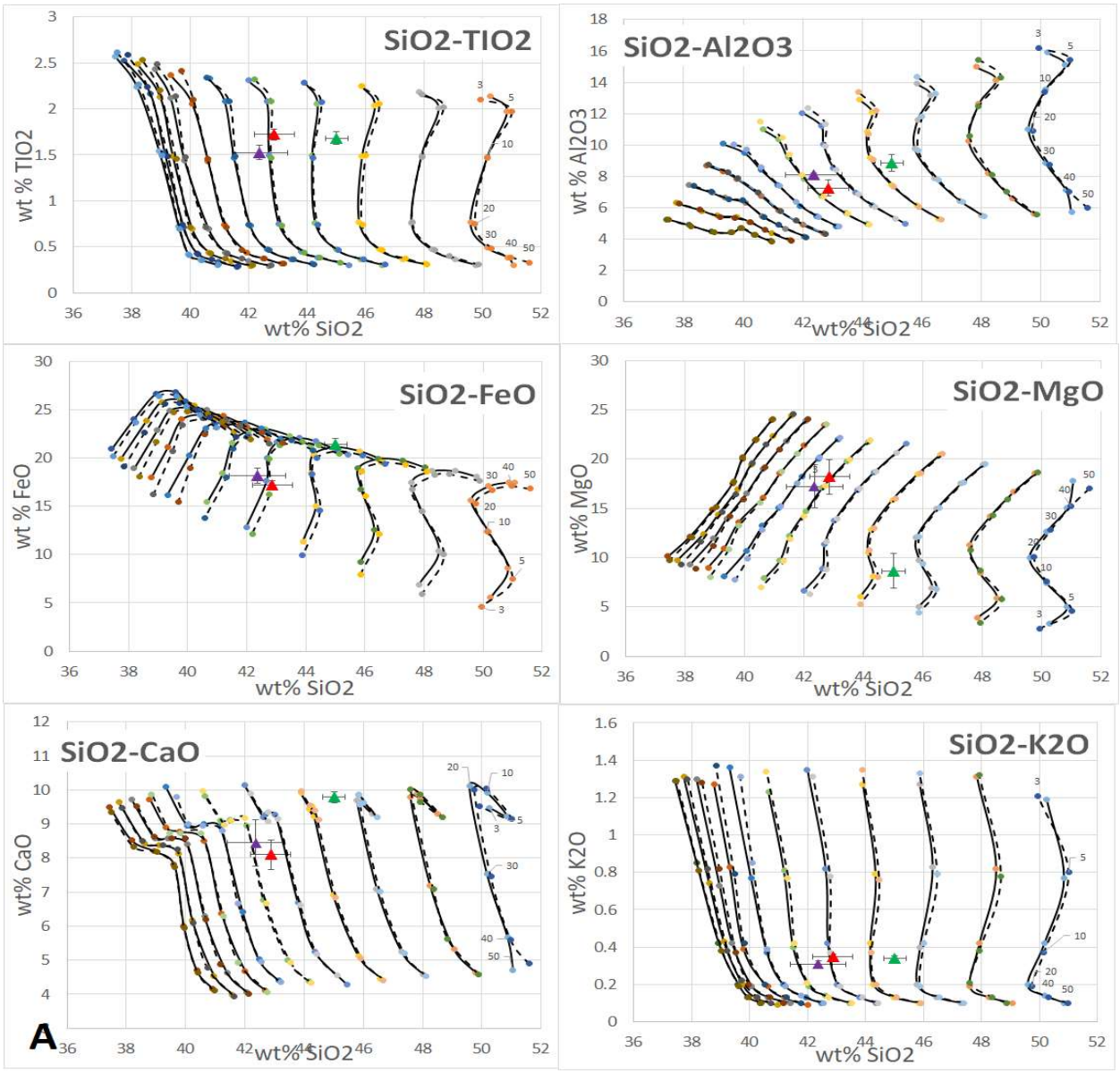

Figure 10. The calculated oxide compositions of the liquids in terms of degree of partial melting, calculated from the pMELTS trials using H2O concentrations of (A) 39 ppm (solid lines) and 185 ppm (dashed lines) and (B) 1800ppm. The appropriate offset corrections calculated from Figure 4 have been added to each oxide. Each curve represents a trial with different initial conditions for pressure. Pressures for this study range from 10kbars to 30kbars in increments of 2 kbars. In all plots, the 10kbars is the curve furthest to the right and progress to the left with increasing pressure creating a "pressure continuum". The number (3, 5, 10, 20, 30, 40, 50) are degrees of partial melting for each trial. Triangles represent the average oxide compositions in each of three Elysium sub-regions. Green represents the SE sub-region, purple represents Central Elysium, and Red represents to NW sub-region. Error bars are calculated from the range of values in each province. (Figure Continued).

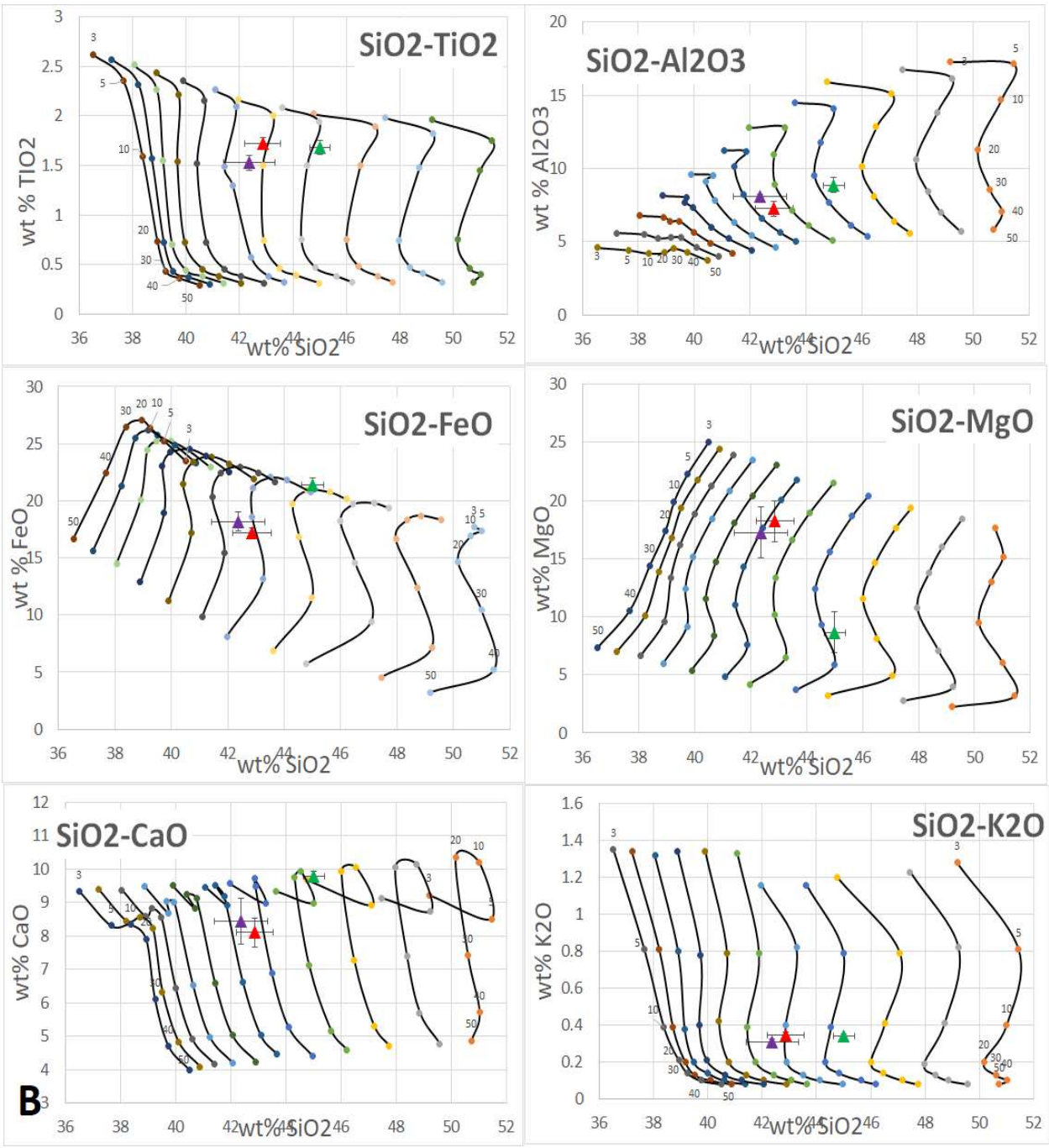

The degrees of partial melting are harder to constrain, showing greater variability across oxides and H_2O contents. The composition of TiO_2 tend to favor low degrees of partial melting for each region with the highest being the Central in the range of 10%. Al_2O_3 on the other hand, favors higher degrees of partial melting for all three sub-regions with the SE at roughly 20% and the NW sub-region with a very large range of possibilities from 20-40%. The FeO plot shows SE with a

higher degree of partial melting (~30%) and the NW and Central with lower values at roughly 5% for the low H_2O content trials and closer to 10% for the high H_2O content case. Interestingly, MgO shows the opposite results of FeO, with the SE closer to 5-10% and the NW and Central regions closer to 25-35%. CaO also places NW and Central in the range of 20-30% and the SE in the range of 5-10%. Last, K_2O shows a range of partial melting between 10 and 20% for all three regions. The visual approximations for pressure and degree of partial melting obtained from Figures 10A and 10B are used to calculate the pressure and depth of melt formation, the mantle potential temperatures for Figures 11 and 12.

While the pressure conditions determined from each oxide are generally consistent, the visual approximation for degree of partial melting varies significantly from oxide-to-oxide. In order to resolve these inconsistencies, I used a second method for calculating partial melting using the ratio of the Th composition of the surface from the GRS data to the Th content of the mantle estimated by the T13 content. This method works under the assumption that Mars has a homogeneous mantle. Since Th is an incompatible element, the abundance of Th in the rock is inversely proportional to degree of partial melting. Consequently this is the same method used to calculate degree of partial melting for various volcanic provinces by Baratoux et al. [2011]. By finding this ratio for each of the three sub-regions, I was able to calculate degrees of partial melting of 13.5±1.3% for SE Elysium, 15.0±1.1% for Central Elysium, and 11.3±0.5% for NW Elysium.

Figure 11 was created by plotting these values against the visual approximations for pressure from Figure 10, with the error bars representing the range of estimated pressures.

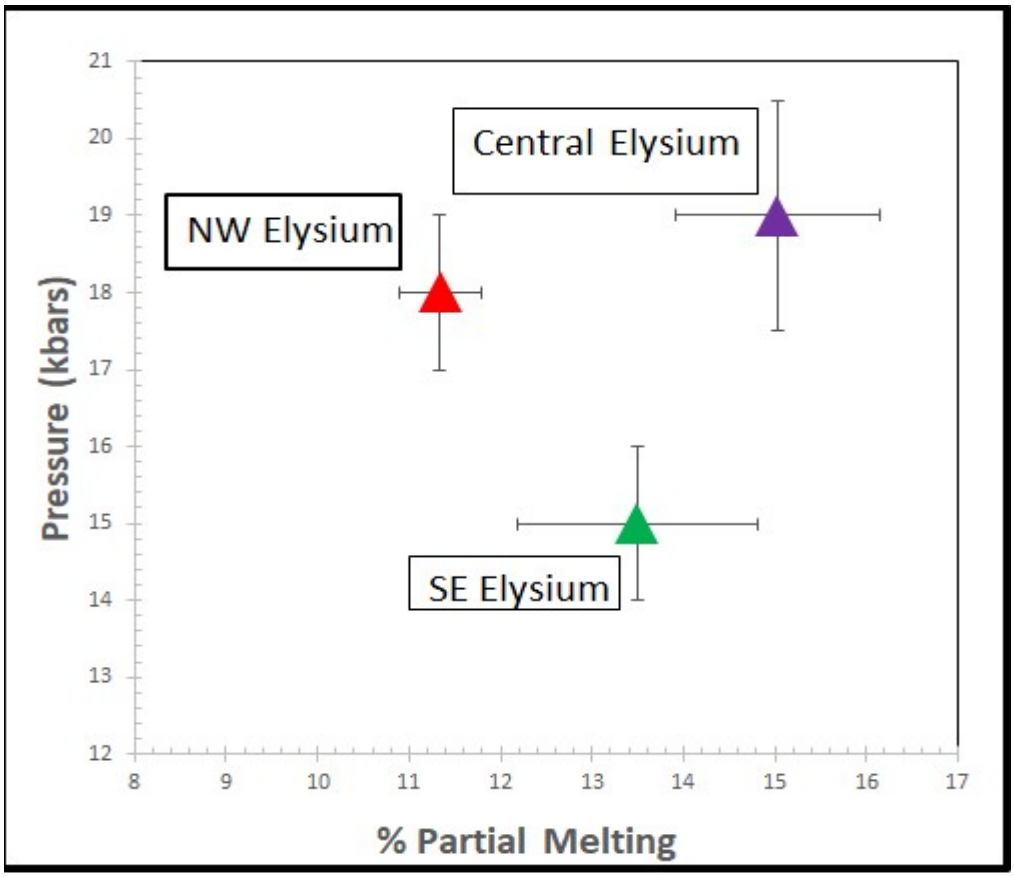

Figure 11. Mantle pressure and degree of partial melting for each of the Elysium sub-regions. The red triangle represents NW Elysium, the purple triangle represents Central Elysium, and the green triangle represents SE Elysium.

From Figure 11, it can be seen that both the mantle pressure and the degree of partial melting increase from the Late Hesperian NW Elysium sub-region to the Early Amazonian Central Elysium sub-region. The pressure and partial melting then decreases from the Central Elysium sub-region to the Late Amazonian SE Elysium region. SE Elysium has a lower mantle pressure than the NW Elysium sub-region, however the degree of partial melting is between the level of the NW and the Central sub-regions.

Central Elysium has the highest mantle potential temperature of any of the three sub-regions, with temperatures of roughly 1470˚C. The NW and SE have similar temperatures to one another, around 1420˚C. The difference between the crustal heat flow of each sub-region is shown by the contours in Figure 12. The NW Elysium sub-region has a crustal heat flow of ~35 mWm^{-2}, the Central sub-region is ~34 mWm^{-2}, and the SE sub-region is ~42 mWm^{-2}. These values help to constrain the properties of the crust-mantle system within the Elysium Volcanic Province.

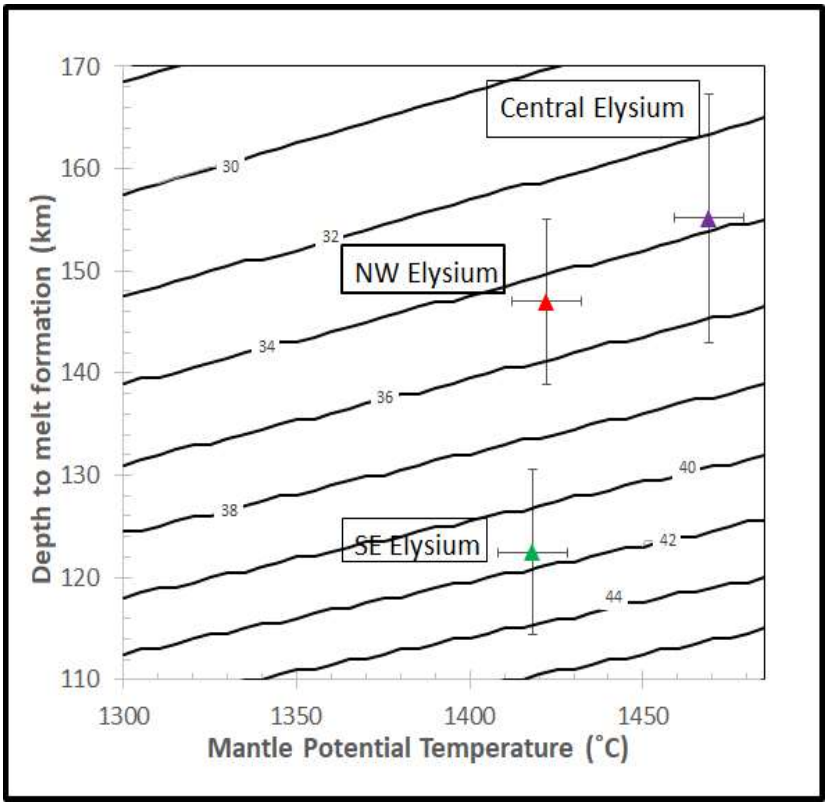

Figure 12. Depth to melting (km) plotted against mantle equilibrium temperature (˚C). Heat flow contour lines in milliwatt per square kilometer are shown. The SE Elysium (green), NW Elysium (red), and Central Elysium (purple) are plotted using the visual approximations from Figure 5. Error bars are calculated using the range of values.

2.4 Discussion and Conclusion

The geochemical analysis and the petrographic modeling completed for this study provide us with insight into the magmatic evolution of the Elysium Volcanic Province. When combined with the results from previous studies, this work makes predictions for how the crust-mantle

system has evolved from the Late Hesperian to the Late Amazonian martian geologic eras. These predictions could have global implications as to the evolution of martian volcanic provinces in general and terrestrial planets that lack tectonic plates.

Figure 7 indicates that each sub-region is chemically distinct, even though each region is dominated by effusive lava flows of similar rheology. Each region is resurfaced with rock from mantle sources with unique conditions, though it does not appear that the trend in geochemistry correlates with the surface age of the region [*Susko et al.*, 2017], indicating that the magmatic evolution is likely more complicated that a monotonic increase in partial melting of the mantle over time.

The TAS diagram is used in this context mostly to compare the Elysium sub-regions with the rest of the martian mid-latitudes and the bulk silicate composition in terms of silica and alkalis. The Elysium sub-regions plot within the picrobasalt and basalt fields, which justifies the use of the QFM-3 oxygen fugacity pathway for the pMELTS simulations. None of the martian meteorites overlap spatially with the Elysium sub-regions.

While pMELTS is effective at determining the initial mantle pressure conditions and the liquid oxide compositions that results from the partial melting of the martian mantle, it is less effective at determining other parameters. The approximated partial melting varies considerably from oxide to oxide. By using the ratio of Th in the surface rocks to the Th content of the mantle, a reasonable degree of partial melting can be calculated for each sub-region. The results from Th content are most consistent with the partial melting estimated from SiO_2-K_2O. This is reasonable since Th and K are both incompatible elements. Last, pMELTS is least effective at predicting H_2O content of the mantle. Results from the pMELTS trial with 39 ppm and 185 ppm are nearly indistinguishable from one another. When the H_2O content is increased by an order of magnitude

to 1800 ppm, it changes each of the resulting oxide compositions in terms of degree of partial melting as seen in Figure 10. However, when considering several other variables at the same time, namely pressure and partial melting, it is difficult to determine which H_2O concentration is most appropriate to apply to the mantle source.

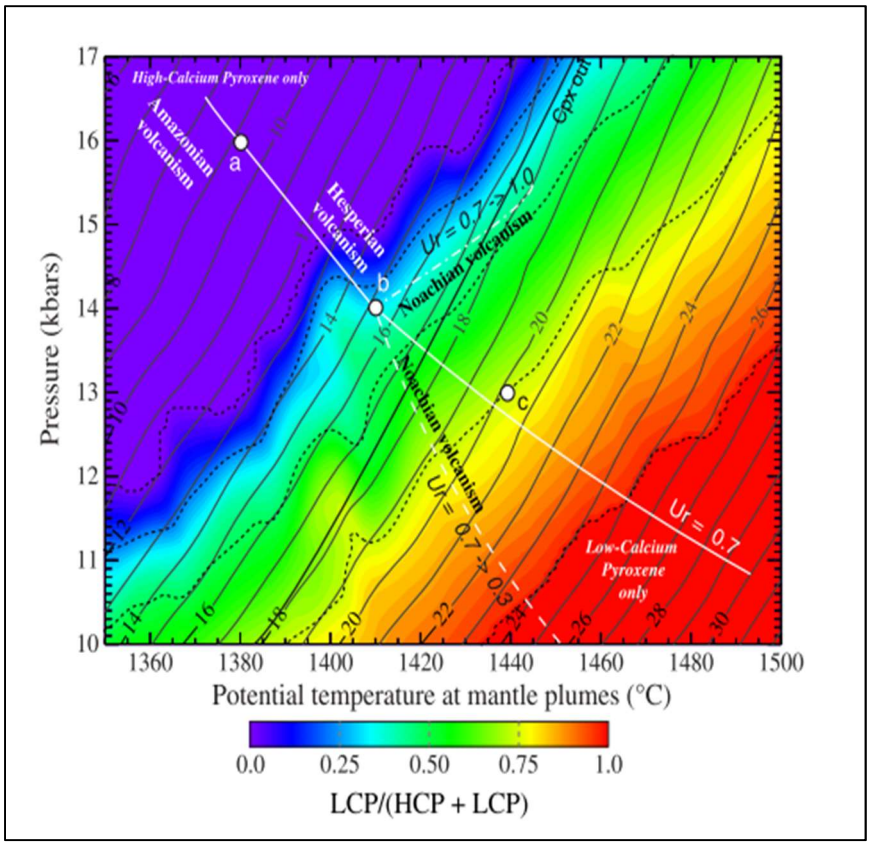

Figure 13. Pyroxene composition as a ratio of Low Calcium Pyroxene (LCP) to High Calcium Pyroxene (HCP) [(LCP)/(HCP+LCP)] as a function of mantle potential temperature and pressure in kbars. Calculated for martian volcanic provinces of Noachian, Hesperian, and Amazonian age using pMELTS. Shows a transition from LCP to HCP over time. This figure is an excerpt from Figure 1 by Baratoux et al. [2013].

The enrichment of CaO in the younger SE Elysium sub-region relative to the older NW could indicate the presence of abundant high-calcium pyroxene (HCP), such as augite [$(Ca,Na)(Mg,Fe,Al,Ti)(Si,Al)_2O_6$] due to the SE region's relative enrichment in Al_2O_3, in the younger volcanic region. In previous studies, this transition was attributed to decreasing mantle potential temperatures for Amazonian magmas [*Baratoux et al.*, 2013]. This interpretation is

consistent with our results from Figure 12, which shows that SE Elysium has the lowest mantle potential temperatures of the three regions. Figure 13 shows the results from pMELTS simulations from a previous study [*Baratoux et al.*, 2013, fig.1], and confirms that the SE Elysium sub-region has mantle potential temperatures and mantle pressures that are consistent with the necessary conditions for HCP to crystalize in the rock.

The depth of melt formation for each sub-region was calculated using the equilibrium pressure, gravitational constant for Mars, and the density of the martian lithosphere (methods) and the results are shown in Figure 12. Of the three sub-regions, the greatest depth to melt formation is within the Central Elysium sub-region (~155±12.2 km), with the NW region being similar though slightly shallower (~147±8 km). The shallowest depth of melt formation is the SE region with a depth of ~122±8 km. Recent work has estimated the thickness of the martian crust in this region with gravity and topographic data [*Genova et al.*, 2016]. This work produced a map of Mars' crustal thickness, which is used in this study to quantify the average thickness of the crust in the Elysium Volcanic Province. The results from the quantification are that the crust in the NW region is 55.6±4.8 km thick, the Central is 46.4±5.2 km, and the SE is 40.0±2.3 km. This means that the melt production for the Elysium Volcanic Province was roughly 92 km beneath the crust of NW Elysium, roughly 110 km beneath Central Elysium, and roughly 82 km beneath the crust of the SE. Figure 12 also shows that the lithosphere of the Elysium Volcanic province has cooled significantly over time. The crustal heat flux is similar for the two sub-regions under the portion of the Elysium Volcanic Province surrounding the Elysium Rise, with values from 33-36 $mW*m^{-2}$ in the late Hesperian NW sub-region and 31-36 $mW*m^{-2}$ in the Early Amazonian Central Elysium sub-region. These values are in agreement with those predicted to support large topographic features on Mars [*McGovern et al.*, 2002; *Belleguic et al.*, 2005]. Interestingly however, the crustal

heat flow increases to ~42 $mW*m^{-2}$ in the Late Amazonian. This is possibly due to the thinner crust in the SE sub-region decreasing the crustal volume through which the heat source in the melt zone of the mantle conducts, relative to the Central and NW sub-regions.

The geochemistry of the Elysium Volcanic Province is consistent with liquid compositions produced by 10-20% partial melting for all three sub-regions and pressures between 17 and 21 kbars for Central Elysium, between 17 and 19 kbars for NW Elysium, and between 14 and 16 kbars for SE Elysium. It is important to note that this is a simplified magmatic model which predicts a single-stage partial melting of the martian mantle without significant contributions from fractional crystallization before eruption on the surface [*El Maarry et al.*, 2009]. These pressures correspond to depths of ~155 km for Central Elysium, ~147 km for NW Elysium, and ~122 km for SE Elysium. Many attempts have been made to estimate the elastic thickness of the martian lithosphere and the variations between various regions, including Elysium. Solomon et al. [1990] predicted a range of possible thicknesses between 48 and 110 km. Later, McGovern et al. [2002] calculated an average elastic lithosphere thickness of 50-80 km for the region. On the other hand, Belleguic et al. [2005], calculated several possible elastic thicknesses for Elysium which might provide more insight into the magmatic history of Elysium. The first estimation neglected subsurface loads and found an elastic thickness of 56±20km. The second estimation is considerably thicker due to the incorporation of subsurface loads. They consider a bottom load located either in the crust as high-density intrusive material or in the mantle as a low-density material. This second estimation had considerably larger uncertainties and only provided an upper bound of 150 km under Elysium Mons.

These estimations are consistent with the interpretation the melt zones calculated by this study are located at the base of the elastic lithosphere in the upper mantle. Furthermore, Belleguic et al. [2005] emphasizes the importance of subsurface loads in the gravity and topography signature from the Elysium Rise. A low density portion of the mantle is interpreted as a result of thermal and compressional effects caused by an active plume in the mantle beneath the Elysium Volcanic Province. The extraction of a partially melted Fe-rich basaltic magma would decrease its density [*Belleguic et al.*, 2005]. This interpretation supports the conclusions by Susko et al. [2017] that the GRS-derived compositions within the Elysium Volcanic Province represent primary magmatism generated from the partial melting of the martian mantle.

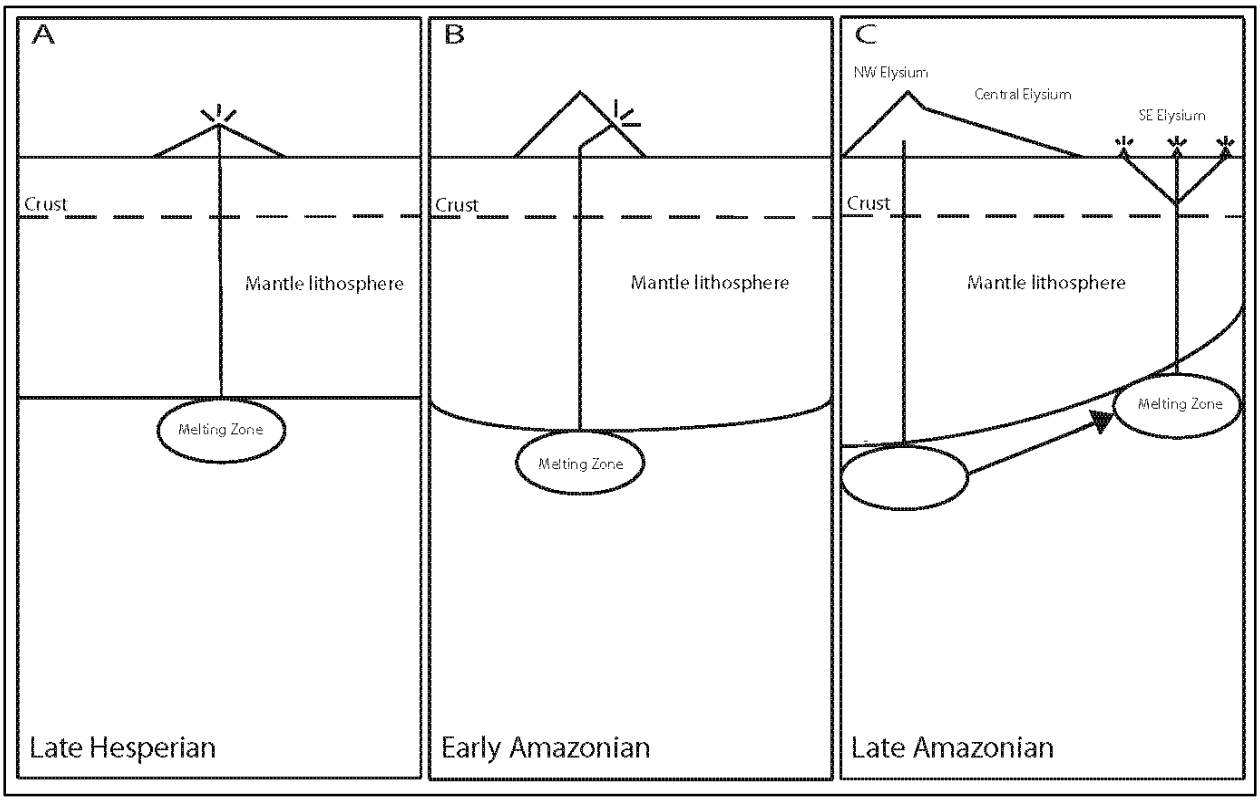

Figure 14. Schematic showing the evolution of the Elysium Volcanic Province from the Late Hesperian to the Late Amazonian. In the late Hesperian, the Elysium Mons edifices form from a source with low partial melting. In the Early Amazonian, the Elysium Rise begins to build as eruptions continue. The lithosphere starts to flex and the pressure increases on the source, and degree of partial melting increases as mantle potential temperatures increase. By the late Amazonian, the lithospheric loading has increased pressure on the original source so much that melt production shuts down. The zone of melt production shifts to the southeast, and volcanism is initiated in SE Elysium.

The results from the modeling support the hypothesis that the variation in surface geochemistry of the Elysium Volcanic Province is largely dependent on a change in depth of melt formation. The oldest exposed resurfacing took place during the Hesperian in the NW Elysium sub-region. As eruptions proceeded to build up the Elysium Rise, the pressure on the mantle beneath the volcanic province increased and the elastic lithosphere began to flex [*Hall et al.*, 1986; *McGovern et al.*, 2002]. This loading is indicated in the region by prominent, concentric grabens which surround the larger volcanic centers. This shutdown melt formation at shallower depths and during the Early Amazonian, the source region increased in both pressure and partial melting. Finally, during the Late Amazonian, mantle pressure became so high that melt formation was shut down at its original source and forced to shift to the southeast, where it initiated eruptions and resurfacing in the SE sub-region. This process is illustrated in Figure 14 and suggests that the magmas which resurfaced the NW and Central sub-regions are generated from the same source, while the SE sub-region has a separate, shallower source.

References

Altheide, T. S., V. F. Chevrier, C. Nicholson, and J. Denson (2009), Experimental investigation of the stability and evaporation of sulfate and chloride brines on Mars, *Earth and Planetary Science Letters*, *282*(1–4), 69–78, doi:10.1016/j.epsl.2009.03.002.

Auzende, A. L., J. Badro, F. J. Ryerson, P. K. Weber, S. J. Fallon, A. Addad, J. Siebert, and G. Fiquet (2008), Element partitioning between magnesium silicate perovskite and ferropericlase: New insights into bulk lower-mantle geochemistry, *Earth and Planetary Science Letters*, *269*(1–2), 164–174, doi:10.1016/j.epsl.2008.02.001.

Balme, M. R., C. J. Gallagher, D. P. Page, J. B. Murray, and J.-P. Muller (2009), Sorted stone circles in Elysium Planitia, Mars: Implications for recent martian climate, *Icarus*, *200*(1), 30–38, doi:10.1016/j.icarus.2008.11.010.

Balta, J. B., and H. Y. McSween (2013a), Application of the MELTS algorithm to martian compositions and implications for magma crystallization, *Journal of Geophysical Research E: Planets*, *118*(12), 2502–2519, doi:10.1002/2013JE004461.

Balta, J. B., and H. Y. McSween (2013b), Water and the composition of Martian magmas, *Geology*, *41*(10), 1115–1118, doi:10.1130/G34714.1.

Baratoux, D., M. J. Toplis, M. Monnereau, and O. Gasnault (2011), Thermal history of Mars inferred from orbital geochemistry of volcanic provinces., *Nature*, *472*(7343), 338–41, doi:10.1038/nature09903.

Baratoux, D., M. J. Toplis, M. Monnereau, and V. Sautter (2013), The petrological expression of early Mars volcanism, *Journal of Geophysical Research E: Planets*, *118*(1), 59–64, doi:10.1029/2012JE004234.

Baratoux, D., H. Samuel, C. Michaut, M. J. Toplis, M. Monnereau, M. Wieczorek, R. Garcia, and K. Kurita (2014), Petrological constraints on the density of the Martian crust, , 1707–1727, doi:10.1002/2014JE004642.

Belleguic, V., P. Lognonné, and M. Wieczorek (2005), Constraints on the Martian lithosphere from gravity and topography data, *Journal of Geophysical Research E: Planets*, *110*(11), 1–22, doi:10.1029/2005JE002437.

Bertka, C. M., and J. R. Holloway (1994), Anhydrous partial melting of an iron-rich mantle II: primary melt compositions at 15 kbar, *Contributions to Mineralogy and Petrology*, *115*(3), 323–338, doi:10.1007/BF00310771.

Boynton, W. V. et al. (2007), Concentration of H, Si, Cl, K, Fe, and Th in the low- and mid-latitude regions of Mars, *Journal of Geophysical Research*, *112*, E12S99, doi:10.1029/2007JE002887.

Burr, D. M., A. S. Mcewen, and S. E. H. Sakimoto (2002a), Recent aqueous floods from the Cerberus Fossae , Mars, *Geophysical Research Letters*, *29*(1), 2–5.

Burr, D. M., J. a Grier, A. S. McEwen, and L. P. Keszthelyi (2002b), Repeated Aqueous Flooding from the Cerberus Fossae: Evidence for Very Recently Extant, Deep Groundwater on Mars, *Icarus*, *159*(1), 53–73, doi:10.1006/icar.2002.6921.

Chevrier, V. F., and T. S. Altheide (2008), Low temperature aqueous ferric sulfate solutions on the surface of Mars, *Geophysical Research Letters*, *35*(22), L22101, doi:10.1029/2008GL035489.

Chevrier, V. F., and E. G. Rivera-Valentin (2012), Formation of recurring slope lineae by liquid brines on present-day Mars, *Geophysical Research Letters*, *39*(21), L21202, doi:10.1029/2012GL054119.

Diez, B., W. C. Feldman, N. Mangold, D. Baratoux, S. Maurice, O. Gasnault, L. D'Uston, and F. Costard (2009), Contribution of Mars Odyssey GRS at Central Elysium Planitia, *Icarus*, *200*(1), 19–29, doi:10.1016/j.icarus.2008.11.011.

Ding, S., and R. Dasgupta (2017), The fate of sulfide during decompression melting of peridotite – implications for sulfur inventory of the MORB-source depleted upper mantle, *Earth and Planetary Science Letters*, *459*, 183–195.

Dohm, J. M. et al. (2008), Recent geological and hydrological activity on Mars: The Tharsis/Elysium corridor, *Planetary and Space Science*, *56*(7), 985–1013, doi:10.1016/j.pss.2008.01.001.

Dreibus, G., and H. Wanke (1985), Mars, a volatile-rich planet, *Journal of Chemical Information and Modeling*, *20*, 367–381, doi:10.1017/CBO9781107415324.004.

Dreibus, G., and H. Wanke (1987), Volatiles on Earth and Mars: A comparison, *Icarus*, *71*(2), Pages 225-240.

Elkins-Tanton, L. T., P. C. Hess, and E. M. Parmentier (2005), Possible formation of ancient crust on Mars through magma ocean processes, *Journal of Geophysical Research E: Planets*, *110*(12), 1–11, doi:10.1029/2005JE002480.

Feldman, W. C., M. T. Mellon, O. Gasnault, B. Diez, R. C. Elphic, J. J. Hagerty, D. J. Lawrence, S. Maurice, and T. H. Prettyman (2007), Vertical distribution of hydrogen at high northern latitudes on Mars: The Mars Odyssey Neutron Spectrometer, *Geophysical Research Letters*, *34*(5), L05201, doi:10.1029/2006GL028936.

Filiberto, J., and R. Dasgupta (2015), Constraints on the depth and thermal vigor of melting in the Martian mantle, *Journal of Geophysical Research E: Planets*, *120*(1), 109–122, doi:10.1002/2014JE004745.

Gaillard, F., J. Michalski, G. Berger, S. M. McLennan, and B. Scaillet (2012), Geochemical Reservoirs and Timing of Sulfur Cycling on Mars, *Space Science Reviews*, *174*(1–4), 251–300, doi:10.1007/s11214-012-9947-4.

Gasnault, O., G. Jeffrey Taylor, S. Karunatillake, J. Dohm, H. Newsom, O. Forni, P. Pinet, and W. V. Boynton (2010), Quantitative geochemical mapping of martian elemental provinces, *Icarus*, *207*(1), 226–247, doi:10.1016/j.icarus.2009.11.010.

Genova, A., S. Goossens, F. G. Lemoine, E. Mazarico, G. A. Neumann, D. E. Smith, and M. T. Zuber (2016), Seasonal and static gravity field of Mars from MGS, Mars Odyssey and MRO radio science, *Icarus*, *272*, 228–245, doi:10.1016/j.icarus.2016.02.050.

Ghosal, S., R. O. Sack, M. E. Lipschutz, and M. S. Ghiorso (1998), Evidence for a reduced, Fe-

depleted martian mantle source region of shergottites, *Contributions to Mineralogy and Petrology*, *130*(3), 346–357.

Grott, M. et al. (2012), Long-Term Evolution of the Martian Crust-Mantle System, *Space Science Reviews*, *174*(1–4), 49–111, doi:10.1007/s11214-012-9948-3.

Hall, J. L., S. C. Solomon, and J. W. Head (1986), Elysium region, Mars; tests of lithospheric loading models for the formation of tectonic features, *JGR. Journal of Geophysical Research. B*, *91*(11), 11,311-377,392.

Hartmann, W. K., and D. C. Berman (2000), Elysium Planitia lava flows' Crater count chronology and geological implications, *Journal of Geophysical Research*, *105*, 15,011-15,025.

Hartmann, W. K., and G. Neukum (2001), Cratering chronology and the evolution of Mars, *Space Science Reviews*, *96*(February), 165–194.

Hirschmann, M. M., M. S. Ghiorso, L. E. Wasylenki, P. D. Asimow, and E. M. Stopler (1998), Calculation of Peridotite Partial Melting from Thermodynamic Models of Minerals and Melts. I. Review of Methods and Comparison with Experiments, *Journal of Petrology*, *39*(6), 1091–1115, doi:10.1093/petrology/39.6.1091.

Hurowitz, J. a., and S. M. McLennan (2007), A ~3.5 Ga record of water-limited, acidic weathering conditions on Mars, *Earth and Planetary Science Letters*, *260*(3–4), 432–443, doi:10.1016/j.epsl.2007.05.043.

Hurowitz, J. A., S. M. McLennan, H. Y. McSween, P. a. DeSouza, and G. Klingelhöfer (2006), Mixing relationships and the effects of secondary alteration in the Wishstone and Watchtower Classes of Husband Hill, Gusev Crater, Mars, *Journal of Geophysical Research*, *111*(E12), E12S14, doi:10.1029/2006JE002795.

Jaeger, W. L., L. P. Keszthelyi, a S. McEwen, C. M. Dundas, and P. S. Russell (2007), Athabasca Valles, Mars: a lava-draped channel system., *Science (New York, N.Y.)*, *317*(5845), 1709–11, doi:10.1126/science.1143315.

Jaeger, W. L., L. P. Keszthelyi, J. A. Skinner, M. P. Milazzo, A. S. McEwen, T. N. Titus, M. R. Rosiek, D. M. Galuszka, E. Howington-Kraus, and R. L. Kirk (2010), Emplacement of the youngest flood lava on Mars: A short, turbulent story, *Icarus*, *205*(1), 230–243, doi:10.1016/j.icarus.2009.09.011.

Jones, E., G. Caprarelli, F. Mills, B. Doran, and J. Clarke (2014), An Alternative Approach to Mapping Thermophysical Units from Martian Thermal Inertia and Albedo Data Using a Combination of Unsupervised Classification Techniques, *Remote Sensing*, *6*(6), 5184–5237, doi:10.3390/rs6065184.

Karunatillake, S., J. M. Keller, S. W. Squyres, W. V Boynton, D. M. Janes, O. Gasnault, and H. E. Newsom (2007), Chemical compositions at Mars landing sites subject to Mars Odyssey Gamma Ray Spectrometer constraints, *Journal of Geophysical Research*, *112*, 1–16, doi:10.1029/2006JE002859.

Karunatillake, S., J. J. Wray, S. W. Squyres, G. J. Taylor, O. Gasnault, S. M. McLennan, W. V. Boynton, M. R. El Maarry, and J. M. Dohm (2009), Chemically striking regions on Mars

and Stealth revisited, *Journal of Geophysical Research*, *114*(E12), E12001, doi:10.1029/2008JE003303.

Karunatillake, S., S. M. McLennan, and K. E. Herkenhoff (2010), Regional and grain size influences on the geochemistry of soil at Gusev crater, Mars, *Journal of Geophysical Research*, *115*, E00F04, doi:10.1029/2010JE003637.

Karunatillake, S., S. W. Squyres, O. Gasnault, J. M. Keller, D. M. Janes, W. V. Boynton, and M. J. Finch (2011), Recipes for Spatial Statistics with Global Datasets: A Martian Case Study, *Journal of Scientific Computing*, *46*(3), 439–451, doi:10.1007/s10915-010-9412-z.

Karunatillake, S., O. Gasnault, S. W. Squyres, J. M. Keller, D. M. Janes, W. V. Boynton, and H. E. Newsom (2012), Martian Case Study of Multivariate Correlation and Regression with Planetary Datasets, *Earth, Moon, and Planets*, *108*, 253–273, doi:10.1007/s11038-012-9395-x.

Karunatillake, S., J. J. Wray, O. Gasnault, S. M. McLennan, A. D. Rogers, S. W. Squyres, W. V Boynton, J. R. Skok, L. Ojha, and N. Olsen (2014), Sulfates hydrating bulk soil in the Martian low and middle latitudes, *Geophysical Research Letters*, *41*(22), 7987–7996, doi:10.1002/2014GL061136.

Kiefer, W. S. (2003), Melting in the martian mantle: Shergottite formation and implications for present-day mantle convection on Mars, *Meteoritics & Planetary Science*, *38*(12), 1815–1832, doi:10.1111/j.1945-5100.2003.tb00017.x.

Leshin, L. A. (2000), Insights into martian water reservoirs from analyses of martian meteorite QUE94201, *Geophysical Research Letters*, *27*(14), 2017–2020, doi:10.1029/1999GL008455.

El Maarry, M. R., O. Gasnault, M. J. Toplis, D. Baratoux, J. M. Dohm, H. E. Newsom, W. V. Boynton, and S. Karunatillake (2009), Gamma-ray constraints on the chemical composition of the martian surface in the Tharsis region: A signature of partial melting of the mantle?, *Journal of Volcanology and Geothermal Research*, *185*(1–2), 116–122, doi:10.1016/j.jvolgeores.2008.11.027.

McCubbin, F. M., E. H. Hauri, S. M. Elardo, Kathleen E. Vander Kaaden, J. Wang, and C. K. S. Jr. (2012), Hydrous melting of the martian mantle produced both depleted and enriched shergottites, *Geology*, *40*(8), 683–686.

McGovern, P. J., S. C. Solomon, D. E. Smith, M. T. Zuber, M. Simons, M. A. Wieczorek, R. J. Phillips, G. A. Neumann, O. Aharonson, and J. W. Head (2002), Localized gravity/topography admittance and correlation spectra on Mars: Implications for regional and global evolution, *Journal of Geophysical Research: Planets*, *107*(E12), 19-1-19–25, doi:10.1029/2002JE001854.

Mckenzie, D., and M. J. Bickle (1988), The volume and composition of melt generated by extension of the lithosphere, *Journal of Petrology*, *29*(3), 625–679, doi:10.1093/petrology/29.3.625.

McSween, H. Y. et al. (2008), Mineralogy of volcanic rocks in Gusev Crater, Mars: Reconciling Mössbauer, Alpha Particle X-Ray Spectrometer, and Miniature Thermal Emission

Spectrometer spectra, *Journal of Geophysical Research*, *113*(E6), 1–14, doi:10.1029/2007JE002970.

McSween, H. Y., G. J. Taylor, and M. B. Wyatt (2009), Elemental composition of the Martian crust., *Science*, *324*(5928), 736–9, doi:10.1126/science.1165871.

McSween, H. Y., I. O. McGlynn, and a. D. Rogers (2010), Determining the modal mineralogy of Martian soils, *Journal of Geophysical Research*, *115*(June), E00F12, doi:10.1029/2010JE003582.

Miller, J. N., and J. C. Miller (2010), *Statistics and Chemometrics for Analytical Chemistry*, 6th ed., Pearson.

Ming, D. W. et al. (2008), Geochemical properties of rocks and soils in Gusev Crater, Mars: Results of the Alpha Particle X-Ray Spectrometer from Cumberland Ridge to Home Plate, *Journal of Geophysical Research*, *113*(E12), E12S39, doi:10.1029/2008JE003195.

Morgan, G. A., B. A. Campbell, L. M. Carter, and J. J. Plaut (2015), Evidence for the episodic erosion of the Medusae Fossae Formation preserved within the youngest volcanic province on Mars, *Geophysical Research Letters*, (Figure 2), 7336–7342, doi:10.1002/2015GL065017.Received.

Murray, J. B., J. Muller, G. Neukum, S. C. Werner, S. Van Gasselt, E. Hauber, W. J. Markiewicz, J. W. H. Iii, and B. H. Foing (2005), Evidence from the Mars Express High Resolution Stereo Camera for a frozen sea close to Mars ' equator, *Letters to Nature*, *434*(March), 352–355.

Nesbitt, H. W. and Wilson, R. E. (1992), Recent chemical weathering of basalts, *American Journal of Science*, *292*, 740–777, doi:10.2475.

Newsom, H. E. et al. (2007), Geochemistry of Martian soil and bedrock in mantled and less mantled terrains with gamma ray data from Mars Odyssey, *Journal of Geophysical Research*, *112*, E03S12, doi:10.1029/2006JE002680.

Ojha, L., M. B. Wilhelm, S. L. Murchie, A. S. McEwen, J. J. Wray, J. Hanley, M. Massé, and M. Chojnacki (2015), Spectral evidence for hydrated salts in recurring slope lineae on Mars, *Nature Geoscience*, (September), doi:10.1038/ngeo2546.

Page, D. P. (2008), Comment on " Athabasca Valles, Mars : A Lava-Draped Channel System," *Science*, *320*(September 2007), 2007–2008, doi:10.1126.

Putzig, N., M. Mellon, K. Kretke, and R. Arvidson (2005), Global thermal inertia and surface properties of Mars from the MGS mapping mission, *Icarus*, *173*(2), 325–341, doi:10.1016/j.icarus.2004.08.017.

Rogers, a. D., and a. H. Nazarian (2013), Evidence for Noachian flood volcanism in Noachis Terra, Mars, and the possible role of Hellas impact basin tectonics, *Journal of Geophysical Research: Planets*, *118*(5), 1094–1113, doi:10.1002/jgre.20083.

Ruff, S. W., and P. R. Christensen (2002), Bright and dark regions on Mars: Particle size and mineralogical characteristics based on Thermal Emission Spectrometer data, *Journal of Geophysical Research*, *107*(E12), 5127, doi:10.1029/2001JE001580.

Sakaia, R., H. Nagaharaa, K. Ozawaa, and S. Tachibanab (2014), Composition of the lunar magma ocean constrained by the conditions for the crust formation, *Icarus*, *229*, 45–56.

Sigurdur R. Gislason, S. A. (1993), Dissolution of primary basaltic minerals in natural waters: saturation state and kinetics, *Chemical Geology*, *105*(1–3), 117–135.

Solomon, S. C., and J. W. Head (1990), Heterogeneities in the Thickness of the Elastic Lithosphere of Mars: Constraints on Heat Flow and Internal Dynamics, *Journal of Geophysical Research*, *95*(B7), 11073–11083.

Spohn, T., Breuer, D. & Johnson, T. (2014), *Encyclopedia of the Solar System, 3rd Edition*, edited by Elsevier.

Susko, D., S. Karunatillake, G. Kodikara, J. R. Skok, J. Wray, J. Heldmann, A. Cousin, and T. Judice (2017), A record of igneous evolution in Elysium, a major martian volcanic province, *Scientific Reports*, *7*, 43177, doi:10.1038/srep43177.

Tanaka, K. L., J. a. Skinner, J. M. Dohm, R. P. Irwin, E. J. Kolb, C. M. Fortezzo, T. Platz, G. Michael, and T. M. Hare (2014a), Geologic Map of Mars, *U.S. Geological Survey Geologic Investigations*, (Pamphlet 43), Map 3292, doi:10.3133/sim3292.

Tanaka, K. L., S. J. Robbins, C. M. Fortezzo, J. a. Skinner, and T. M. Hare (2014b), The digital global geologic map of Mars: Chronostratigraphic ages, topographic and crater morphologic characteristics, and updated resurfacing history, *Planetary and Space Science*, *95*, 11–24, doi:10.1016/j.pss.2013.03.006.

Taylor, G. J. (2013), The bulk composition of Mars, *Chemie der Erde - Geochemistry*, *73*(4), 401–420, doi:10.1016/j.chemer.2013.09.006.

Taylor, G. J. et al. (2006), Variations in K/Th on Mars, *Journal of Geophysical Research*, *112*(E3), E03S06, doi:10.1029/2006JE002676.

Taylor, G. J., L. M. V. Martel, S. Karunatillake, O. Gasnault, and W. V. Boynton (2010), Mapping Mars geochemically, *Geology*, *38*(2), 183–186, doi:10.1130/G30470.1.

Thurber, C. H., and M. N. Toksoz (1978), Martian Lithospheric Thickness from Elastic Flexure Theory, *Geophysical Research Letters*, *5*(11), 977–980.

Vaucher, J., D. Baratoux, N. Mangold, P. Pinet, K. Kurita, and M. Grégoire (2009), The volcanic history of central Elysium Planitia: Implications for martian magmatism, *Icarus*, *204*(2), 418–442, doi:10.1016/j.icarus.2009.06.032.

Yen, A. S. et al. (2005), An integrated view of the chemistry and mineralogy of Martian soils., *Nature*, *436*(7047), 49–54, doi:10.1038/nature03637.

Vita

David Susko is a Master's student at Louisiana State University (LSU) studying geology with a focus in planetary science, remote sensing, and martian igneous processes. He has been working in planetary science since January 2014, when he was an undergraduate student working with Dr. Suniti Karunatillake in the LSU Planetary Science Laboratory (PSL). He completed an undergraduate thesis titled *Exploring the History of the Martian Volcano Elysium and Developing an Instrument to Discover Subsurface Martian Ice.* This undergraduate thesis would eventually lay the foundation for his graduate research as a Master's student.

David graduated in August 2015, and continued his research in the PSL as a graduate student. During this time, he successfully identified a history of variable magmatic compositions within the Elysium Volcanic Province and successfully published his work as a peer-reviewed paper in the *Scientific Reports* journal. David also published a manuscript as a co-author with a fellow PSL graduate student on the Greater Thaumasia Plateau of Mars in the *Journal of Geophysical Research*. David has also garnered considerable experience in proposing to funding venues. In the Spring of 2016, he proposed to the Louisiana Space Grant Consortium and won the Graduate Student Research Assistantship (GSRA).

David plans on continuing his career in planetary science by continuing his education to the PhD level. Over the past few years interest has peaked in space resource acquisition and utilization. Both government organizations and several private enterprises have begun looking to become involved in the creation of an industry. After completing a PhD, David intends on pursuing a career as a planetary scientist with one of the space resource companies, including: Deep Space Industries, Planetary Resources, Moon Express, or Shackleton Energy Company, or pursue a postdoctoral position at a research institution.